Extracellular matrix-driven metabolic control of pancreatic endocrine lineage allocation

Christine Ebeid^{1,4,7}, Adam Rump ^{1,2,5,7}, Chenglei Tian ^{1,2}, Anant Mamidi ^{1,6}, Adèle De Arcangelis ^{1,3}, Gérard Gradwohl ^{1,0} & Henrik Semb ^{1,2} ⊗

Abstract

The mechanical and metabolic states of progenitor and stem cells are emerging as key regulators of cell fate decisions. Lineage specification of pancreatic endocrine cells is promoted by reduced mechanical tension in vitro, but the underlying mechanism is poorly understood. Here, we show that heterogeneously deposited lowadhesion extracellular matrix (ECM) components, such as the laminin isoform LN411, trigger a local "soft" environment by broadly reducing the expression of integrins. Mimicking this lowtension state by in vitro knockdown and in vivo gene targeting of the LN-binding integrins Itaa3 and Itaa6 reveal their importance in inducing endocrinogenesis. Unexpectedly, the cell responds to this change in tensile forces by engaging a major metabolic enzyme, PDK4, to execute the resulting cell fate decision. PDK4 achieves this through two distinct mechanisms: a non-canonical action controlling YAP activity and a canonical metabolic function maintaining PDX1 expression. In sum, we believe our findings have broad relevance for how local changes in mechanical tension governs cell behaviour in many developmental and disease contexts.

Keywords Pancreatic Endocrinogenesis; PDK4; Laminin-411;
Mechanotransduction; YAP Signalling
Subject Categories Cell Adhesion, Polarity & Cytoskeleton; Development;

https://doi.org/10.1038/s44319-025-00610-6

Received 25 March 2025; Revised 25 September 2025;

Accepted 13 October 2025

Published online: 27 October 2025

Introduction

Recent advances in single-cell RNA sequencing have significantly enhanced our understanding of the gene regulatory networks governing cell fates (Asp et al, 2019; La Manno et al, 2021; Olaniru et al, 2023). However, much less is known about the identity and mechanisms of the environmental cues that control the fate-inducing transcriptional machinery. Here, we unravel the identity and mode of action of important niche cues that control the gene

regulatory apparatus involved in the differentiation of the endocrine cell lineages during pancreas development.

During pancreas development, the epithelium is segregated into a pro-acinar "tip" and a bipotent ductal/endocrine compartment. Endocrine progenitor cells are specified in a salt and pepper pattern within the bipotent epithelium by induction of the transcription factor Neurog3 (Apelqvist et al, 1999; Gu et al, 2002; Gradwohl et al, 2000). However, our understanding of the identity and functional mechanisms of the extracellular cues that induce differentiation of endocrine progenitors remains incomplete. A lateral inhibition mechanism has been proposed to control Neurog3 induction, wherein Neurog3 upregulates the Notch ligand Dll1 to repress Neurog3 expression in neighboring cells (Qu et al, 2013). However, the expression patterns of both Notch ligands and the key Notch target gene Hes1 are inconsistent with a classical lateral inhibition model (Ahnfelt-Rønne et al, 2012). An alternative model is thus needed to explain how a small, scattered subset of bipotent pancreatic progenitor cells is specified toward the endocrine lineage.

Recently, we and others identified YAP-mediated mechanosignalling as an upstream regulator of Notch signaling during development of the pancreas and a variety of other tissues (Mamidi et al, 2018; Engel-Pizcueta and Pujades, 2021; Cebola et al, 2015). While YAP activity is classically regulated by the Hippo pathway, the mild phenotype of pancreas-specific Hippo component knockout suggests Hippo-independent regulation during pancreas development (Mamidi et al, 2018; Gao et al, 2013). Recent work revealed extensive Hippo-independent regulation of YAP activity by the extracellular matrix (ECM), actin dynamics, and cellular metabolism (Panciera et al, 2017; Chi et al, 2020; Ibar and Irvine, 2020). Consistently, we demonstrated that confinement of pancreatic bipotent progenitors in vitro, for example via certain ECM molecules or actin depolymerization, promotes endocrine specification through reduced YAP activity (Mamidi et al, 2018). However, what remains unclear is whether this machinery is operational in vivo, and by which environmental signal it is controlled.

Recent studies have demonstrated that metabolic pathways play key roles in the regulation of cell fates. For instance, glucose metabolism controls the first lineage segregation during

¹Novo Nordisk Foundation Center for Stem Cell Biology (DanStem), University of Copenhagen, Copenhagen 2200, Denmark. ²Institute of Translational Stem Cell Research, Helmholtz Diabetes Center, Helmholtz Zentrum München, Neuherberg 85764, Germany. ³Institut de Génétique et de Biologie Moléculaire et Cellulaire, CNRS UMR 7104/INSERM U1258/Université de Strasbourg, Illkirch 67404, France. ⁴Present address: Cell Therapy R&D, Novo Nordisk A/S, Måløv 2760, Denmark. ⁵Present address: Chemometec A/S, Allerød 3450, Denmark. ⁶Present address: FUJIFILM Diosynth Biotechnologies, Hillerød 3400, Denmark. ⁷These authors contributed equally: Christine Ebeid, Adam Rump. ⁵⁵⁵ Femail: henrik.semb@helmholtz-munich.de

mammalian development by regulating YAP nuclear localization through the hexosamine biosynthetic pathway, thereby specifying trophectodermal fate (Chi et al, 2020). This metabolic control extends to major developmental transitions, as demonstrated by mannose metabolism directing mesoderm specification during gastrulation (Cao et al, 2024). However, while these studies establish metabolism as a key regulator of development, both the roles of specific metabolic regulators in organ-specific cell fate decisions and the way in which these regulators are influenced by environmental cues remain largely unexplored.

In this study, the low adhesion LN411 is identified as the key extrinsic regulator of endocrine fate choice. LN411 adhesion leads to reduced expression of integrins, including the laminin-binding integrins $\alpha 3$ and $\alpha 6$, in bipotent progenitor cells. We show that in vitro knockdown and in vivo knockout of these integrins increase endocrine induction. Hence, heterogeneous deposition of LN411 within the trunk epithelium may explain why a subset of bipotent pancreatic progenitor cells adopt an endocrine fate.

Surprisingly, we identify the metabolic regulatory kinase PDK4, which regulates conversion of pyruvate to acetyl-CoA (Holness and Sugden, 2003), as a key mediator of LN411-induced endocrine specification. Specifically, exposure to LN411 induces upregulation of *PDK4*, which induces endocrinogenesis through dual functions. While YAP is inhibited by a non-canonical mechanism, *PDX1* expression is maintained via reduced production of acetyl-CoA. Altogether, our findings provide a new paradigm for how cells integrate mechanosignalling and metabolism to control cell fate decisions.

Results

LN411 induces endocrine specification of pancreatic progenitors

We previously showed that plating pancreatic progenitors on human placenta laminin induces their endocrinogenesis (Mamidi et al, 2018). To pinpoint which laminin isoform is most potent in inducing endocrinogenesis in vitro, we reseeded human embryonic stem cell (hESC)-derived pancreatic progenitors from the HUES4 cell line on nine different laminin isoforms. The extent of endocrine induction was notably contingent on the specific laminin isoform, with LN211 and LN411 being the most effective inducers of NEUROG3, insulin, and glucagon expression (Fig. 1A-D). Importantly, while both LN211 and LN411 showed strong endocrinogenic effects in the HUES4 cell line, only the effect of LN411 was conserved in the independent SA121-derived NEU-ROG3 reporter (NGN3-GFP) hESC cell line (Fig. EV1A-C). This cell line-independent effect led us to focus our subsequent mechanistic studies on LN411. Interestingly, the endocrinogenic effect by LN211 and LN411 was associated with cell clustering, whereas cells reseeded on fibronectin and the other laminin isoforms spread form monolayer to (Figs. 1A and EV1A and EV2A,B). As anticipated from our previous model of laminin-induced endocrine specification, LN411 induced decreased levels of actin polymerization, nuclear YAP, and expression of YAP target genes (Fig. EV2C,D). Collectively, these findings underscore a distinct and specific pro-endocrinologic effect of LN411 in vitro across multiple cell lines.

LN411 induces endocrinogenesis via reduced cell-ECM adhesion

LN411 has previously been shown to have lower adhesion properties compared to other laminin isoforms (Ishikawa et al, 2014). This decreased adhesion has been shown to impact the surface expression of integrins, as weak binding of integrins to the ECM disrupts focal adhesion and stress fiber formation, leading to integrin internalization (Du et al, 2011). Consistently, we found a coordinated reduction in the expression of both fibronectinbinding integrins $\alpha 5$ and αV and laminin-binding integrins $\alpha 3$ and α6 at both the RNA and protein levels upon exposure to LN411 (Figs. 2A and EV3A). To assess whether the decreased expression of integrins is directly associated with endocrinogenesis, we examined the expression of each integrin in NGN3-GFP+ hESCs upon latrunculin B treatment (Mamidi et al, 2018). Indeed, the expression of each of the four integrins was reduced in NGN3-GFP+ endocrine progenitors compared to their NGN3-GFPcounterparts (Fig. EV3B,C). These findings suggest that LN411 induces endocrinogenesis via a reduction in cell-ECM adhesion.

To ascertain whether the reduced expression of integrins by LN411 is secondary to increased endocrine induction, we measured the expression of each integrin 3, 6, or 24 h after reseeding. Remarkably, the expression of each integrin was reduced at every time point. At 6 h after reseeding, the expression of *ITGA6*, *ITGA5* and *ITGAV* was significantly reduced, while there was no difference in the expression of any endocrine marker gene at this time point (Fig. 2B). This indicates that reduced expression of integrins precedes endocrine induction upon reseeding on LN411.

To genetically validate the direct role of integrin $\alpha 3$ and $\alpha 6$ in endocrinogenesis, siRNA-based knockdown experiments were performed. Knockdown of either integrin $\alpha 3$ or $\alpha 6$ was sufficient to enhance endocrine specification (Fig. 2C,D). Importantly, this enhancement occurs when cells are cultured on LN521, precluding a specific effect of LN411-integrin interactions. These findings collectively demonstrate that reduced expression of laminin-binding integrins $\alpha 3$ and $\alpha 6$ actively promotes endocrine specification, thus providing compelling evidence for a mechanistic link between LN411-induced reduction in cell-ECM adhesion and the induction of endocrine fate in pancreatic progenitors.

Reduced expression of laminin-binding integrins promotes endocrinogenesis in vivo

To validate our in vitro findings in vivo, we analyzed the consequences of knocking out integrins $\alpha 3$ and $\alpha 6$ in the developing mouse pancreas. First, we examined the distribution of laminin isoforms in the pancreatic epithelium at E15.5, which revealed a heterogenous distribution of laminin $\alpha 4$ (Fig. EV4). Due to the previously reported functional redundancy between *Itga3* and *Itga6*, we generated single and double knockouts by intercrossing *Itga3*^{+/-} and *Itga6*^{+/-} mice (De Arcangelis et al, 1999). Given the embryonic lethality of the double knockouts, we conducted the analysis using an ex vivo explant system (Fig. 3A).

Knockout of either *Itga3* or *Itga6* alone had no discernible effects on pancreas size, morphology, or proportion of endocrine cells (Fig. 3D). However, the pancreas of the *Itga3/Itga6* double knockouts exhibited an expansion of the endocrine compartment, coupled with hypoplasia and reduced branching (Fig. 3B–D). A

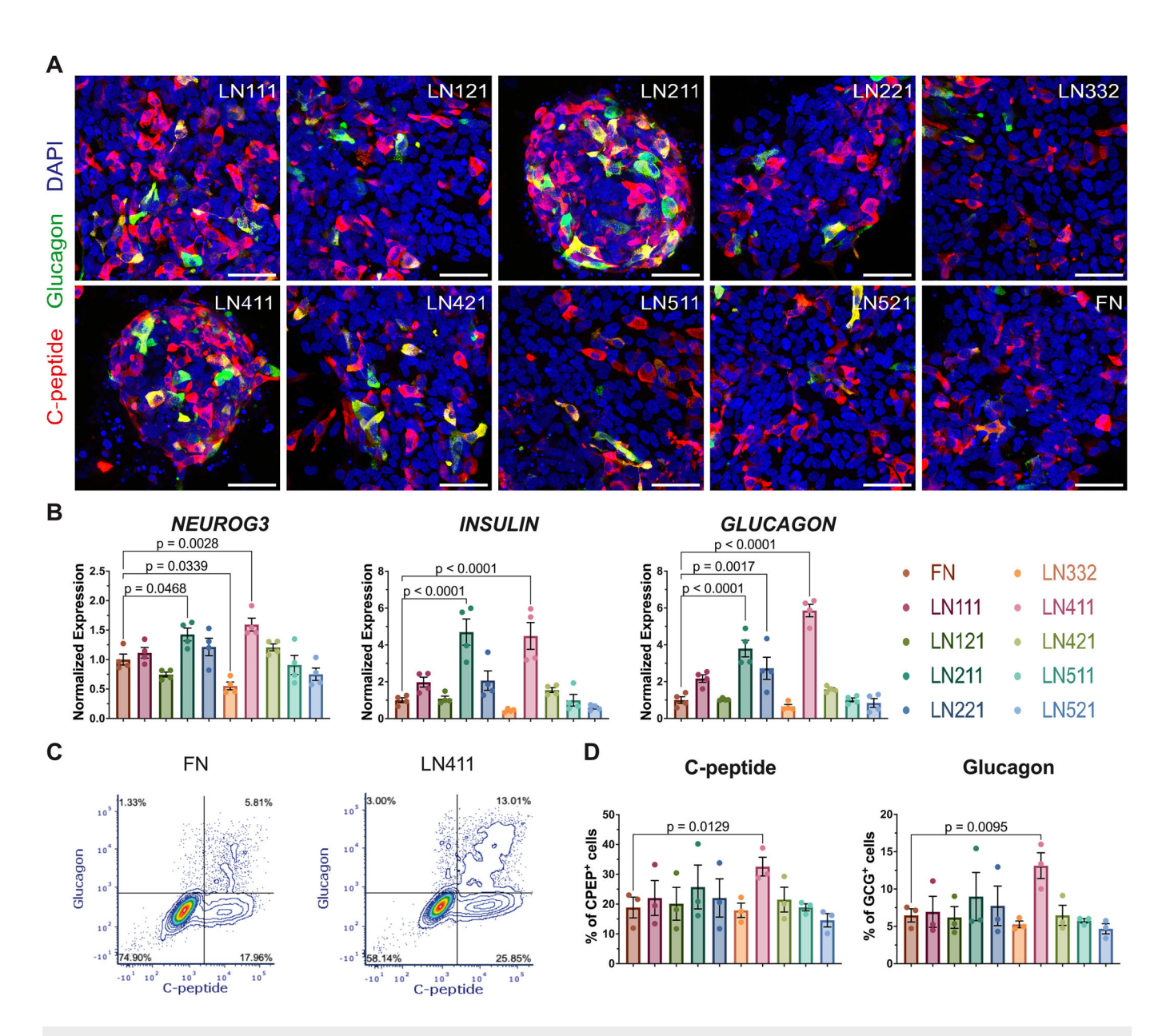


Figure 1. LN411 specifically induces endocrine specification.

(A) Maximum intensity projection images of HUES4-derived pancreatic progenitors reseeded on indicated ECM proteins for 9 days. Immunofluorescence with DAPI (blue), glucagon (green), and C-peptide (red). Scale bar = $50 \mu m$. (B) qPCR analysis of endocrine marker genes (*NEUROG3, INSULIN*, and *GLUCAGON*) 4 days after reseeding on indicated ECM proteins. The data were analyzed by Dunnett's test with comparison to FN and are shown as mean expression \pm SEM (n=4, biological replicates). (C) Representative flow cytometry plots of C-peptide and Glucagon expression 9 days after reseeding on the indicated ECM proteins. (D) Quantification of total C-peptide positive cells and Glucagon positive cells in (C). The data were analyzed by Dunnett's test with comparison to FN and are shown as mean expression \pm SEM (n=3, biological replicates). Source data are available online for this figure.

similar phenotype of pancreatic hypoplasia coupled with expansion of the endocrine compartment occurs in the pancreata of Yap1 or Hes1 knockout mice (Mamidi et al, 2018; Jensen et al, 2000). In the case of Hes1 knockout, this phenotype has been attributed to premature specification of post-mitotic endocrine cells (Jensen et al, 2000). Together, these findings indicate that reduced expression of the laminin-binding integrins hinders the expansion of pancreatic bipotent progenitors and promotes their differentiation into the endocrine lineage over the duct lineage in a functionally redundant manner.

Reduced cell-ECM adhesion induces endocrine specification via *PDK4*

To unravel the downstream targets responsible for the endocrinogenic impact of reduced cell-ECM adhesion, we carried out a time course bulk RNA sequencing of bipotent pancreatic progenitor cells reseeded on LN411 or fibronectin for 3, 6, or 24 h. At 3 h, only 67 genes were differentially expressed, increasing to 1065 genes at 6 h and 5780 genes at 24 h. Genes involved in endocrine specification such as *NEUROG3*, *NEUROD1*, *INSM1*, and *NKX2-2* were all only

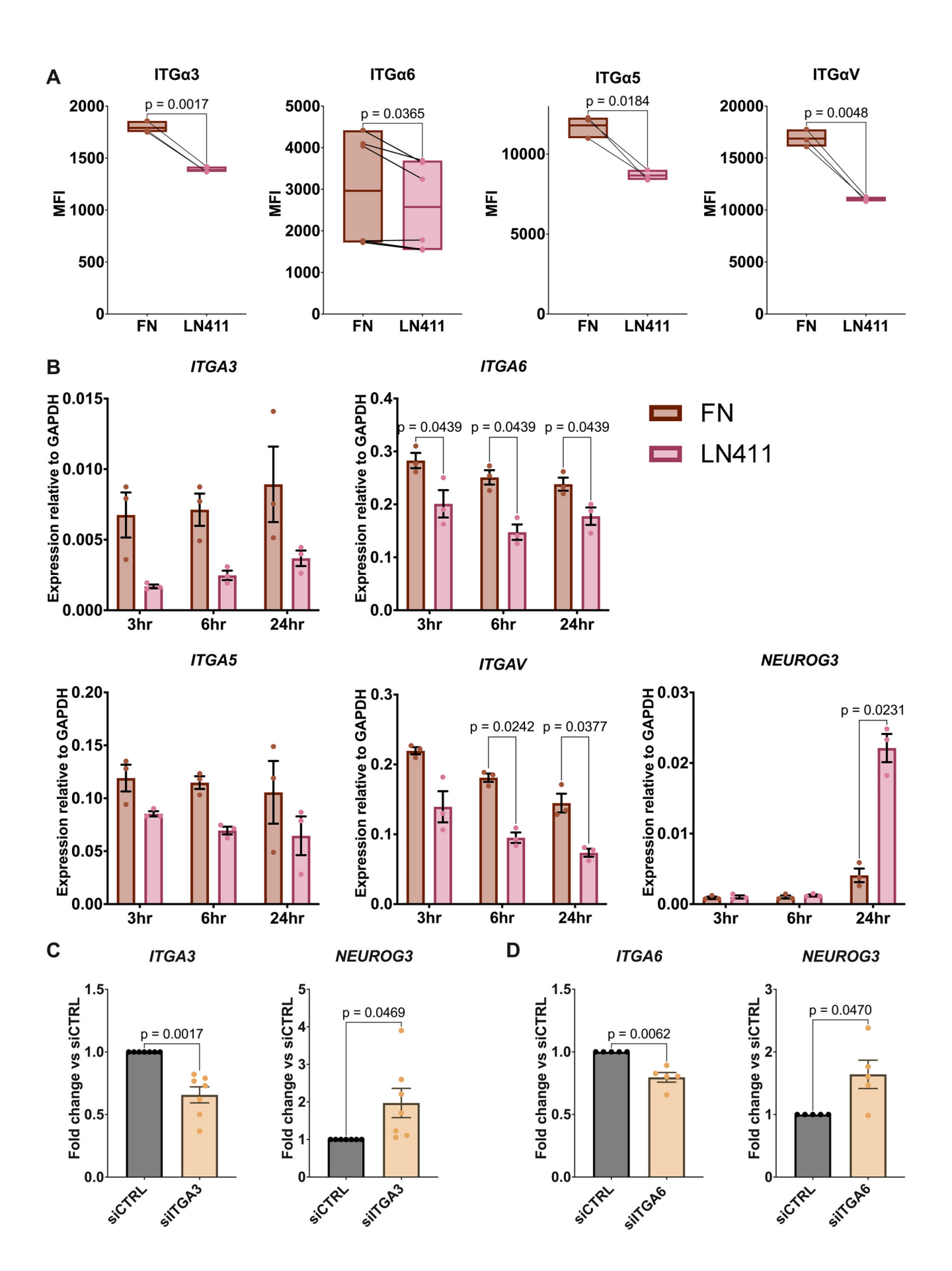


Figure 2. LN411 induces endocrine specification downstream of integrin downregulation.

(A) Flow cytometry analysis of surface expression of indicated integrins 2 days after reseeding of NGN3-GFP-derived pancreatic progenitors on FN or LN411. Data were analyzed by two-tailed paired t-tests and are shown as boxplots with box boundaries extending to the minimum and maximum with a line at the mean (n = 6 for ITG α 6, n = 3 for ITG α 5, ITG α 5, and ITG α 7, biological replicates). (B) qPCR analysis of cell-ECM adhesion genes (ITG α 6, ITG α 7, ITG α 8, and ITG α 9) and the endocrine marker gene NEUROG3 at indicated time points after reseeding on LN411 or FN. The data were analyzed by paired t-tests with Holm-Šídák adjustment for multiple comparisons and are shown as mean expression α 5 SEM (α 6, α 7, biological replicates). (C) qPCR analysis of ITG α 8 and NEUROG3 2 days after transfection of pancreatic progenitors with siRNA targeting ITG α 8. The data were analyzed using two-tailed paired t-tests and are shown as mean expression α 8 SEM (α 7, biological replicates). (D) qPCR analysis of ITG α 8 and NEUROG3 2 days after transfection of pancreatic progenitors with siRNA targeting ITG α 8. The data were analyzed using two-tailed paired t-tests and are shown as mean fold change in expression α 9. Self (α 1, α 2, biological replicates). (D) qPCR analysis of ITG α 8.

significantly upregulated after 24 h, with a minor increase in *NEUROG3* expression at an earlier time point (Fig. 4A). Consistent with previous findings demonstrating YAP-mediated enhancement of endocrinogenesis upon inhibition of actin polymerization (Mamidi et al, 2018; Hogrebe et al, 2020), key YAP targets, including *CYR61* (*CCN1*) and *CTGF* (*CCN2*), were significantly downregulated after 6 h of treatment (Fig. 4A). A similar pattern of reduced expression of YAP targets at 6 h without an increase in expression of endocrine marker genes was observed after treatment of cells with the actin-depolymerizing agent latrunculin B (Fig. EV5A).

Both LN411 exposure and latrunculin B treatment led to endocrine specification via reduced actin polymerization. LN411 acts upstream by downregulating cell-ECM adhesion, while latrunculin B directly targets actin polymerization. In both cases, YAP target genes are downregulated already at 6 h, while induction of endocrine genes is delayed. This pattern indicates the presence of previously unidentified intermediate steps in the regulation of the endocrinogenic transcriptional program. We thus hypothesized that comparing the differentially expressed genes in the latrunculin B and LN411 sequencing datasets would reveal key genes involved in the shared endocrinogenic program, while treatment-specific effects unrelated to the endocrinogenic program would be filtered out.

Of the top 100 significantly upregulated genes in each condition only nine overlapped (DDIT4, FOXA3, MET, MAN1A1, FST, FOXP1, RGS4, PDK4, and RFX6) (Fig. 4B). While FST, FOXP1, RGS4 and RFX6 have been associated with pancreatic development (Miralles et al, 1998; Spaeth et al, 2015; Serafimidis et al, 2011; Smith et al, 2010; Soyer et al, 2010), their known roles make them unlikely candidates for mediating actin depolymerization-induced endocrine specification. Specifically, FST has been shown to downregulate rather than upregulate endocrine induction (Miralles et al, 1998), while RFX6, RGS4, and FOXP1 function downstream of NEUROG3 in general endocrine development, delamination, and αcell function, respectively (Smith et al, 2010; Serafimidis et al, 2011; Spaeth et al, 2015). In contrast, DDIT4, MAN1A1, and PDK4 have not previously been implicated in pancreas development. The decrease in PDK4 expression upon ECM attachment (Grassian et al, 2011) and its identification as a mediator of anchorageindependent growth (Tambe et al, 2019) indicate its potential significance as a relevant target for further investigation.

PDK4 encodes pyruvate dehydrogenase kinase 4, a protein serine kinase that inhibits the key metabolic enzyme pyruvate dehydrogenase, which in turn controls the conversion of pyruvate to acetyl-CoA (Zhang et al, 2014). Interestingly, *PDK4* expression increased while key YAP target genes *CYR61* (*CCN1*) and *CTGF*

(CCN2) decreased prior to NEUROG3 upregulation during both latrunculin B-treatment (3 h) and LN411 exposure (6 h) (Figs. 4A and EV5A).

Upregulation of PDK4 expression upon exposure to LN411 was validated using qPCR and Western blotting (Fig. EV5B-D). siRNAbased knockdown of PDK4 mRNA resulted in the downregulation of NEUROG3, thus providing genetic evidence for the functional role of PDK4 in endocrinogenesis (Fig. 4C). Consistently, treatment of bipotent pancreatic progenitor cells with the pan-PDK inhibitor dichloroacetate (DCA) reduced the expression of NEUROG3 and NEUROD1 after reseeding on LN411 (Fig. 4E) as well as without reseeding (Fig. EV5F). These effects were validated using the GFP reporter in the NGN3-GFP cell line (Figs. 4D and EV5E). Interestingly, treatment with DCA did not alter the cell morphology upon reseeding on LN411 (Fig. 4D), suggesting that cell aggregation is a consequence of upstream events, rather than a consequence of endocrinogenesis. Altogether, these data demonstrate that PDK4 is a novel effector of the cell-ECM adhesion/actin cytoskeleton-mediated regulation of endocrine specification.

PDK4 controls endocrine specification via maintaining PDX1 expression and inducing NEUROG3 expression

To examine whether *PDK4* regulates endocrine specification via YAP (Mamidi et al, 2018; Hogrebe et al, 2020), we assessed the impact of DCA treatment on YAP activity. Upon reseeding cells on LN411, DCA treatment induced higher nuclear concentrations of YAP in NKX6-1⁺ bipotent progenitor cells (Fig. 5A,B). This was accompanied by higher expression of the YAP target genes *CYR61* and *CTGF* (Fig. 5C). A similar upregulation was observed in unreseeded cells following DCA treatment (Fig. EV5G). Altogether, these data indicate a key role of *PDK4* in mediating reduced YAP-activity downstream of reduced cell-ECM adhesion.

To address whether PDK4 controls YAP activity via a non-canonical (Thoudam et al, 2022; Lee et al, 2022a) or metabolic mechanism, we treated pancreatic progenitors with acetate. Acetate can readily be converted into acetyl-CoA, thereby bypassing a conceivable non-canonical mechanism by PDK4. Akin to DCA treatment, acetate abrogated the expression of *NEUROG3* and *NEUROD1* (Figs. 6A,B and EV6A,B). However, acetate failed to increase nuclear YAP intensity in NKX6-1⁺ bipotent progenitor cells (Fig. 6C,D). Consistently, the expression changes of YAP target genes were marginal, with a small increase in the expression of *CTGF* counterbalanced by a small decrease in the expression of *CYR61* (Fig. 6E). Collectively, these findings indicate that PDK4 induces endocrinogenesis through both YAP-independent metabolic and YAP-dependent non-canonical mechanisms.

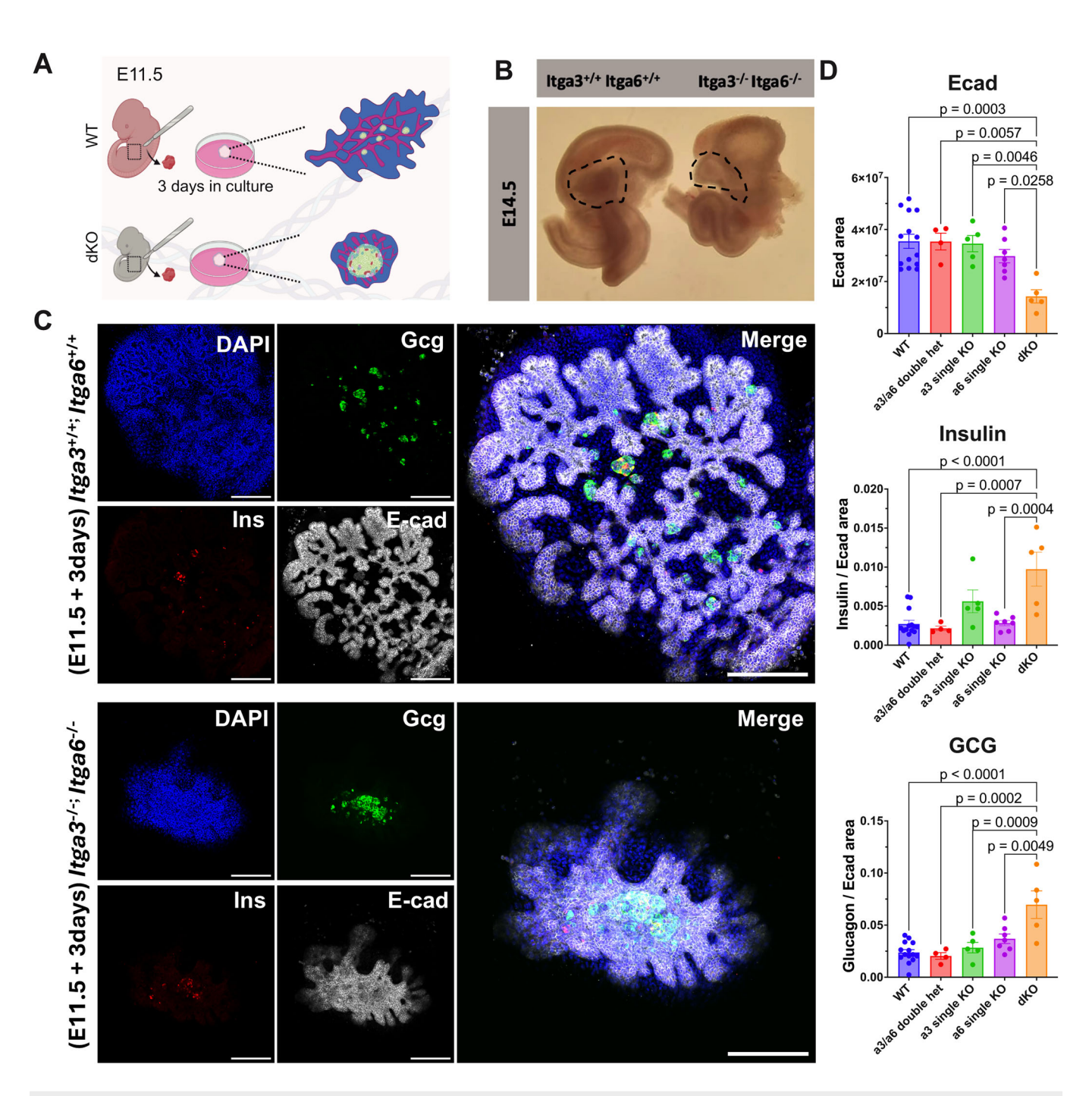


Figure 3. ITGA3 and ITGA6 redundantly inhibit endocrine specification in vivo.

(A) Schematic of the explant experimental setup. Due to embryonic lethality of $ltga3^{-/-}$; $ltga6^{-/-}$ mouse embryos, pancreata were explanted at E11.5. Explants were then cultured for 3 days, after which hypoplasia was apparent in double knockout explants. (B) Images showing part of the dissected gastrointestinal tract from E14.5 WT and $ltga3^{-/-}$; $ltga6^{-/-}$ mouse embryos. The double knockout exhibits hypoplasia of the pancreas (outlined). (C) Representative whole-mount staining of $ltga3^{+/-}$ / $ltga6^{+/-}$ pancreata explanted at E11.5 and cultured for 3 days ex vivo. Immunostaining with DAPI (blue), insulin (red), glucagon (green), and E-cadherin (E-cad, White). Scale bar = 200 µm. (D) Quantification of the staining for $ltga3^{+/-}$ / $ltga6^{-/-}$ and $ltga3^{-/-}$ / $ltga6^{+/-}$ pancreatic explants. The data were analyzed by Tukey's test and are shown as mean expression \pm SEM (n = 14 for wild type, 4 for double heterozygotes, 7 for ltga6 single knockout, and 5 for ltga3 single knockout and ltga3/ltga6 double knockout, biological replicates). Source data are available online for this figure.

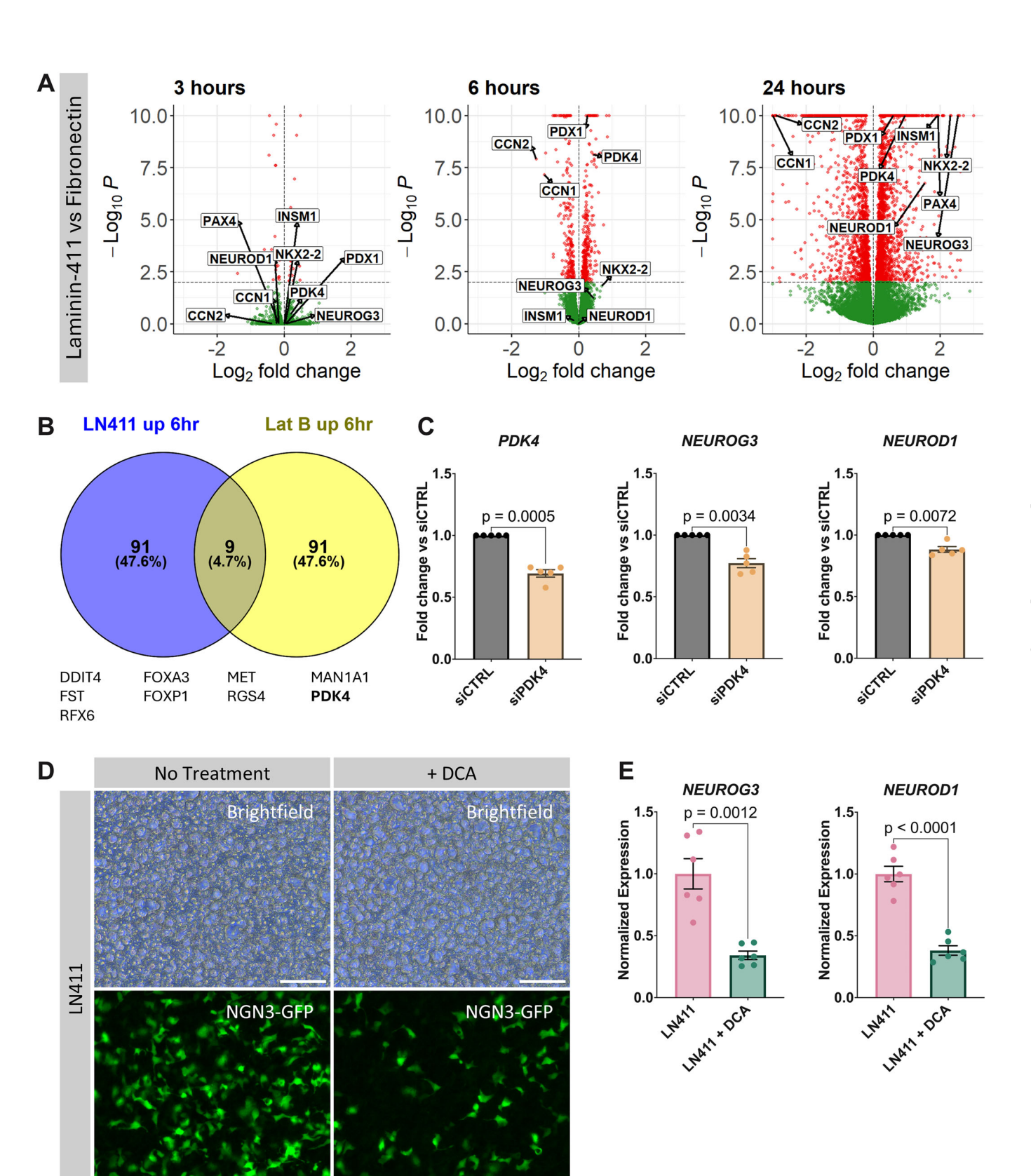


Figure 4. LN411 induces endocrine specification via PDK4.

(A) Volcano plots of bulk RNA-seq analysis of NGN3-GFP-derived pancreatic progenitors reseeded on LN411 or FN at the indicated time points. Expression of YAP target genes (CCN1/CYR61, CCN2/CTGF), early endocrine genes (NEUROG3, NEUROD1, INSM1, NKX2-2), PDX1 and PDK4 are indicated. Differential expression analysis was performed using DESeq2 (n=3, biological replicates). (B) Venn diagram of the top 100 upregulated genes by significance at 6 h after reseeding on LN411 (compared to reseeding on FN) or treatment with latrunculin B (LatB) (compared to before treatment). (C) qPCR analysis of PDK4, and endocrine marker genes (NEUROG3 and NEUROD1) 2 days after transfection with siRNA targeting PDK4. The data were analyzed using two-tailed paired t-tests and are shown as mean fold change in expression \pm SEM (n=6, biological replicates). (D) Brightfield (top panels) and epifluorescence (bottom panels) images of NGN3-GFP derived pancreatic progenitor cells 2 days after reseeding on LN411 with or without treatment with 10 mM DCA. High-density regions form a web-like structure rather than discrete circular aggregates. Scale bar = 100 μ m. (E) qPCR analysis of endocrine marker genes NEUROG3 and NEUROD1 in pancreatic progenitors 2 days after reseeding on LN411 with or without 10 mM DCA treatment. The data were analyzed using two-tailed paired t-tests and are shown as mean expression \pm SEM (n=6, biological replicates). Source data are available online for this figure.

We previously observed that confinement of individual pancreatic progenitors not only reduced YAP expression and increased NEUROG3 expression, but also maintained PDX1 expression, suggesting a role of PDK4 in sustaining PDX1 expression during endocrinogenesis (Mamidi et al, 2018). Indeed, LN411 exposure increased PDX1 expression alongside PDK4 prior to enhanced NEUROG3 expression (Fig. 4A). The fact that both DCA and acetate reduced PDX1 expression suggest an involvement of PDK4 via its metabolic function (Figs. 6F and EV6D). This was corroborated by decreased intracellular levels of acetyl-CoA prior to increased NEUROG3 expression. As expected, the LN411-mediated reduction of acetyl-CoA was blocked by concurrent treatment with acetate or DCA (Fig. EV6E).

Taken together, these findings indicate that PDK4 controls endocrine specification through two mechanisms: (1) maintenance of PDX1 expression via YAP-independent reduction of acetyl-CoA (canonical) and (2) induction of NEUROG3 via a YAP-dependent mechanism (non-canonical)(Mamidi et al, 2018) (Figs. 6G and EV7).

To assess the relevance of our findings to human in vivo development, we analyzed previously published single-cell RNA sequencing datasets. We focused on the OMIX001616 dataset of human fetal pancreata covering weeks 4–11 post conception (wpc) (Ma et al, 2023), and restricted the analysis to 8–10 wpc when a well-defined trunk population giving rise to endocrine progenitor cells was present (Zhang et al, 2025; Ma et al, 2023).

Consistent with our in vitro findings, endocrine progenitors showed significant downregulation of genes encoding integrins $\alpha 3$, $\alpha 6$, $\alpha 5$, and αV compared to bipotent trunk progenitors, validating reduced cell-ECM adhesion during endocrine specification (Fig. EV8A). These cells also exhibited significant upregulation of PDX1 and a trend toward increased PDK4 expression, alongside the previously described downregulation of YAP target genes (Fig. EV8A).

We further assessed laminin expression in the human fetal pancreas using a broader dataset including both epithelial and non-epithelial cells (Olaniru et al, 2023). *LAMA4* expression peaked at 8–10 wpc (Fig. EV8B), coinciding with the onset of endocrine induction (Ma et al, 2023; Zhang et al, 2025). Importantly, *LAMA4* expression was largely restricted to non-epithelial cells, with high expression levels in Schwann and endothelial cells and moderate expression in mesenchymal cells, making these cells the likely source of LN411 during pancreatic development (Fig. EV8B). These findings validate the gene expression changes of our proposed pathway components at the onset of endocrinogenesis during human pancreas development in vivo, with expression of *LAMA4*

at the appropriate developmental window alongside the expected decreased expression of integrins and increased expression of *PDK4* and *PDX1* in endocrine progenitor cells.

Altogether, these findings delineate a pathway linking ECM composition to endocrine fate choice via integrated mechanical and metabolic signaling pathways. First, LN411 exposure induces a broad-based downregulation of integrins $\alpha 3$, $\alpha 6$, $\alpha 5$ and αV , leading to reduced cell-ECM adhesion and actin depolymerization. This triggers *PDK4* upregulation, which specifies endocrine fate via noncanonical YAP inhibition and metabolically mediated *PDX1* upregulation (Fig. 6G).

Discussion

It is well-established that cell fate decisions can be regulated by cell-ECM interactions and cellular metabolism (Mahmoud, 2023; Chi et al, 2020; Dingare et al, 2024), and that cell-ECM adhesion modulates cellular metabolism (Romani et al, 2020). However, there are no known examples of metabolic mediators mediating ECM-guided cell fate decisions. Here, we provide a new mechanism for how mechanosignaling via cell-ECM adhesion controls cell fate decisions via a metabolic regulator of glycolysis. We arrived at this conclusion by studying how endocrinogenesis in the developing pancreas is regulated by environmental influences.

Previous work demonstrated that tensile forces govern cell fate decision of bipotent pancreatic progenitors towards either an endocrine or duct fate (Mamidi et al, 2018). Here, we identify reduced cell-ECM adhesion as a major inducer of endocrinogenesis. Unexpectedly, we find that LN411 causes reduced cell-ECM adhesion through a rapid global reduction of the transcription and surface expression of multiple integrins. Thus, it is a broad lowering of integrin expression rather than targeting of specific integrin receptor-ligand signaling that triggers a mechanical cellular state conducive to endocrinogenesis. Another unknown aspect is how alterations in mechanical tension are transduced via the actin cytoskeleton into the pro-endocrinogenetic reduction in YAP signaling. Here, we identify a key metabolic kinase, PDK4, as a central player in transducing changes in cell-ECM adhesion into transcriptional regulation of endocrinogenesis. Interestingly, our results indicate that PDK4 regulates endocrinogenesis through both non-canonical and canonical mechanisms. Whereas the former represents the previously identified YAP-regulated pathway (Mamidi et al, 2018), the latter corresponds to a newly identified metabolically mediated pathway. Specifically, our findings suggest

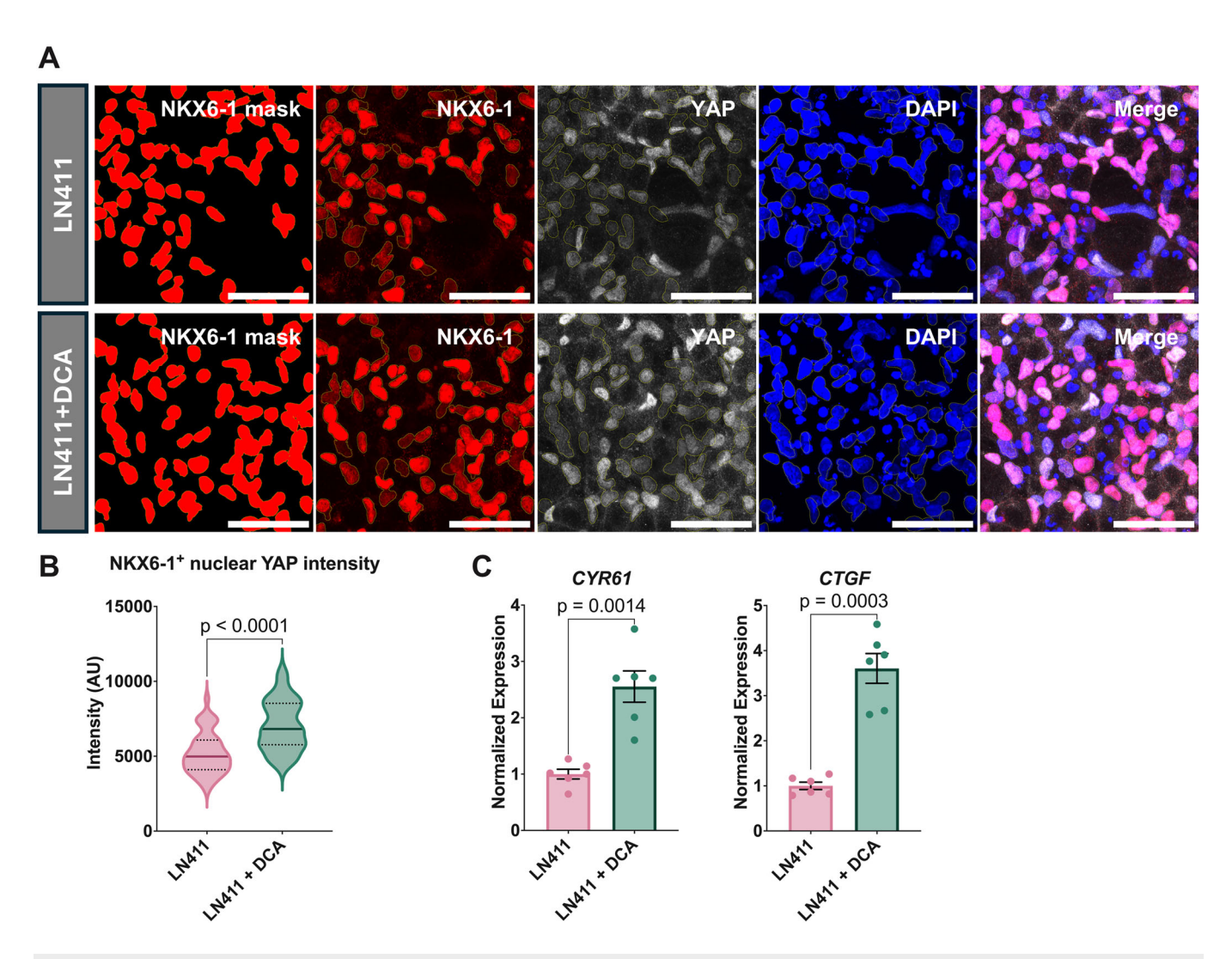


Figure 5. The PDK4-inhibitor DCA inhibits endocrine specification via activation of YAP.

(A) Representative maximum intensity projections of NGN3-GFP-derived pancreatic progenitor cells 1 day after reseeding on LN411 with or without 20 mM DCA. A mask of NKX6-1⁺ nuclei generated using llastik is shown in the first panel. Immunofluorescence for NKX6-1 (red), YAP (white), and DAPI (blue). Scale bar = 50 μ m. (B) Quantification of nuclear YAP expression in 312 NKX6-1⁺ nuclei from four independent replicates (176 without DCA and 136 with DCA treatment). The data were analyzed using a two-tailed Welch's *t*-test. (C) qPCR analysis of the YAP target genes *CYR61* and *CTGF* in pancreatic progenitors 2 days after reseeding on LN411 with or without 10 mM DCA. The data were analyzed using two-tailed paired *t*-tests and are shown as mean expression \pm SEM (n = 6, biological replicates). Source data are available online for this figure.

that PDK4 maintains PDX1 expression via reduced levels of acetyl-CoA (Fig. 6G).

The physiological relevance of our model is supported by gene expression analysis of human pancreatic development, where endocrine progenitors exhibit downregulation of *ITGA3*, *ITGA6*, *ITGA5*, and *ITGAV* and upregulation of *PDX1* and *PDK4*. The observed pattern of up- and downregulated genes in vivo perfectly matches the pattern observed during our mechanistic in vitro studies. Further, a peak in *LAMA4* expression at 8–10 wpc coincides with the timing of the onset of endocrinogenesis in vivo. Altogether, this in silico analysis supports our model that heterogeneous LN411 deposition drives local endocrine fate decisions during normal human development.

In mature human and murine islets, LN411 is deposited in the vascular basement membrane, and the main source is pericytes

(Sakhneny et al, 2021). During development, LN411 is known to be secreted by a subset of endothelial cells and by Schwann cells in the developing pancreas (Frieser et al, 1997; Olaniru et al, 2023). Single cell analysis of human pancreatic development confirms that both Schwann cells and endothelial cells express *LAMA4* at high levels during the onset of endocrinogenesis at 8–10 wpc (Olaniru et al, 2023). Schwann cells have recently been shown to co-localize with endocrine progenitor cells during human pancreas development (Olaniru et al, 2023). Whether Schwann cells play a functional role during pancreas development remains to be investigated. Existing data regarding the role of endothelial cells in endocrinogenesis is conflicting. While hypervascularization and endothelial cell depletion studies demonstrated a positive influence on endocrinogenesis by endothelial cells (Lammert et al, 2001; Pierreux et al, 2010), other studies identified mechanisms by

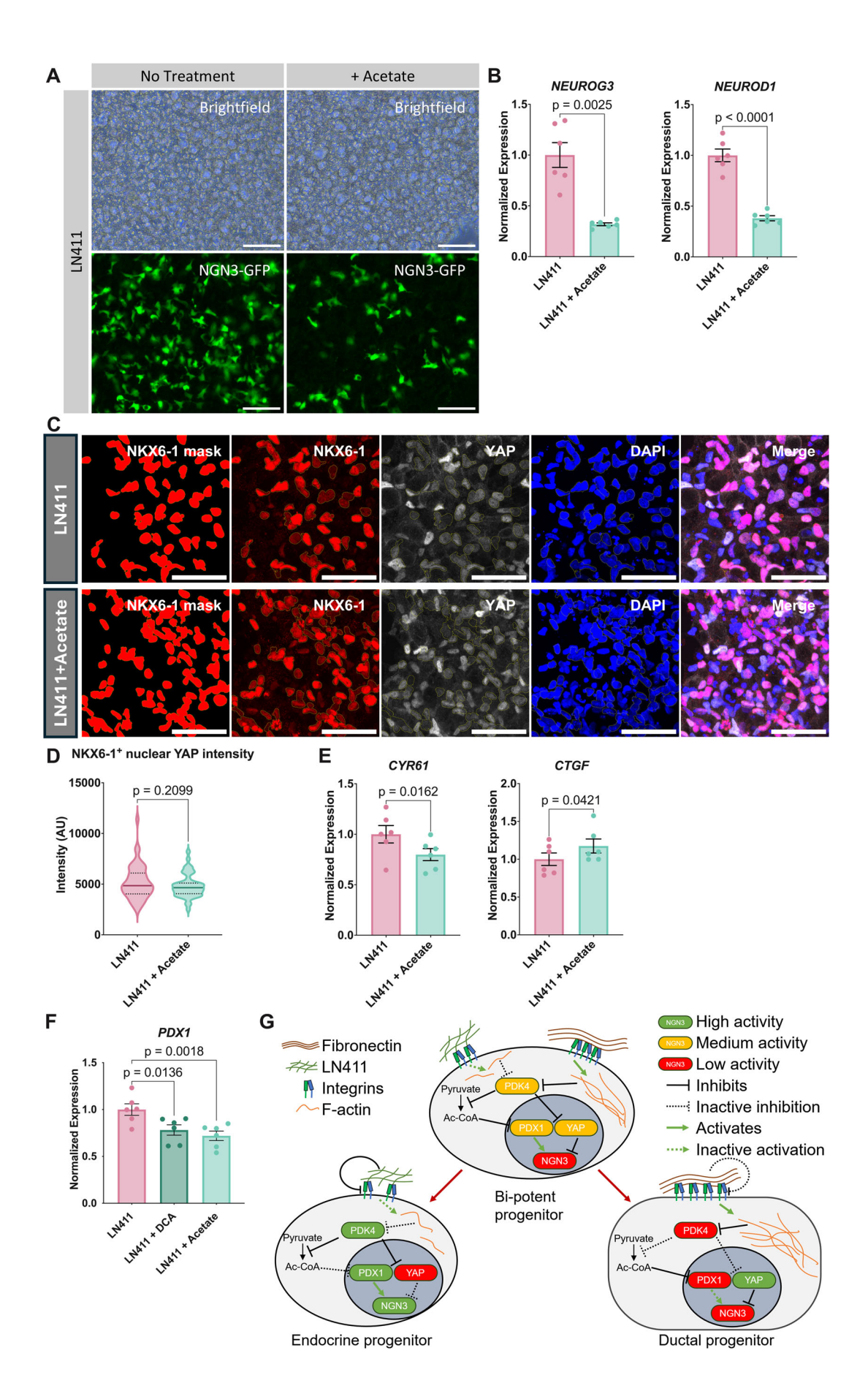


Figure 6. Acetate inhibits endocrine specification via a YAP-independent mechanism.

(A) Brightfield (top panels) and epifluorescence (bottom panels) images of pancreatic progenitors 2 days after reseeding on LN411 with or without 10 mM sodium acetate treatment. (B) qPCR analysis of endocrine marker genes *NEUROG3* and *NEUROD1* in pancreatic progenitors 2 days after reseeding on LN411 with or without 10 mM sodium acetate treatment. The data are shown as mean expression ± SEM (n = 6, biological replicates). (C) Representative maximum intensity projections of NGN3-GFP derived pancreatic progenitors 1 day after reseeding on LN411 with or without 10 mM sodium acetate treatment. A mask of NKX6-1+ nuclei generated using llastik is shown in the first panel. Immunofluorescence for NKX6-1 (red), YAP (white), and DAPI (blue). Scale bar = 50 µm. (D) Quantification of nuclear YAP expression in 253 NKX6-1+ nuclei from three independent replicates (127 without sodium acetate and 126 with sodium acetate treatment). The data were analyzed using a two-tailed Welch's t-test. (E) qPCR analysis of the YAP target genes *CYR61* and *CTGF* in pancreatic progenitor cells 2 days after reseeding on LN411 with or without 10 mM sodium acetate treatment. The data were analyzed using two-tailed paired t-tests and are shown as mean expression ± SEM (n = 6, biological replicates). (F) qPCR analysis of *PDX1* expression in pancreatic progenitors 2 days after reseeding on LN411 with or without 10 mM acetate or DCA. The data were analyzed by Dunnett's test compared to LN411 alone and are shown as mean expression ± SEM (n = 6, biological replicates). (G) Model depicting the role of ECM, integrins, and PDK4 in endocrine fate choice. Exposure to LN411 induces downregulation of integrins on both the protein and RNA levels. This is turn reduces the level of actin polymerization and leads to disinhibition of *PDK4* expression. PDK4 inhibits the generation of acetyl-CoA and YAP activity. Reduced levels of acetyl-CoA promote maintenance of *PDX1* expression. The combination of YAP inhibition and high *PDX1* expression permits the expre

which endothelial cells inhibit endocrinogenesis (Magenheim et al, 2011; Kao et al, 2015).

Other examples of cell-ECM adhesion-mediated control of cell fate decisions via mechanical cues have been reported. For example, LN411 plays a role in the specification of retinal lineages during ocular development (Shibata et al, 2018), and of endothelial cell identity (Hall et al, 2022; Ohta et al, 2016). Although LN411's effect on endothelial cell differentiation is dependent on focal adhesion kinase, integrin-linked kinase, Notch and β -catenin signaling, the crosstalk between these pathways remains to be determined (Hall et al, 2022). Given YAP's strong connection with the Notch (Totaro et al, 2018) and Wnt signaling pathways (Azzolin et al, 2014), it is worth considering whether the LN411-PDK4-YAP axis uncovered in this study also plays a role during endothelial development.

Core metabolic enzymes often regulate cellular processes beyond their enzymatic activity—a phenomenon often referred to as "moonlighting" (Lu and Hunter, 2018). An example is PKM2, which is an isoform of the enzyme that controls the generation of pyruvate from phosphoenolpyruvate. This enzyme is part of the core glycolytic machinery but also regulates a wide range of other cellular processes through its non-canonical kinase activity, including gene expression, histone modification, mitosis, and apoptosis (Lee et al, 2022b). Here, we provide another example of the moonlighting phenomenon in which PDK4 contributes to the induction of endocrinogenesis through its non-canonical control of YAP activity. Exploring the mechanism by which PDK4 regulates YAP forms an interesting avenue for future research. One possibility is through the previously described regulation of Septin-2 by PDK4 (Thoudam et al, 2022). Septin-2 is involved in the mechanical control of YAP, specifically by being required for increased YAP activity on stiff substrates (Calvo et al, 2015).

Ample evidence supports a requirement for PDX1 in endocrinogenesis (Fujitani et al, 2006; Oliver-Krasinski et al, 2009; Zhu et al, 2016). For example, PDX1 hypomorphisms are associated with defective development of the endocrine pancreas in mice (Oliver-Krasinski et al, 2009) and human patients (Nicolino et al, 2010), suggesting that maintenance of PDX1 expression is required for endocrinogenesis in mice and man. We have previously demonstrated a strong relationship between LN-mediated cell confinement/soft environment and PDX1 expression (Mamidi et al, 2018). Based on the previously established inverse relationship between FOXA2 acetylation and PDX1 expression (Wang et al, 2013), we speculate that locally reduced cell-ECM adhesion

maintains high PDX1 expression through PDK4-mediated reduction of FOXA2 acetylation through lowered acetyl-CoA synthesis from pyruvate.

Thus, the identification of PDK4 as a regulator of YAP and PDX1 via non-canonical and canonical mechanisms, respectively, highlights the need for considering the interplay between ECM-mediated mechanosignalling and metabolism in future studies of cell fate decisions of stem cells/progenitors during organogenesis.

Methods

Reagents and tools table

Reagent/resource	Reference or source	Identifier or catalog number	
Experimental models			
C57BL/6 (M. musculus)	In house	NA	
Itga3 ^{+/-} ; Itga6 ^{+/-} mice (M. musculus)	De Arcangelis et al, 1999	MGI:1857792 MGI:1857793	
NGN3-GFP (SA121) ES cells (H. sapiens)	Löf-Öhlin et al, 2017	NA	
HUES4 ES cells (H. sapiens)	Harvard University	BioSamples: SAMEA114214019	
Antibodies			
Anti-insulin (1:400)	DAKO	#A0564 RRID:AB_10013624	
Anti-E-cadherin (1:400)	Takara	#M108 RRID:AB_2895157	
Anti-glucagon (1:1000)	Sigma	#G2654 RRID:AB_259852	
Anti-ITGA3 (1:100)	R&D	#AF2787 RRID:AB_2129595	
Anti-ITGA6 (1:200)	Millipore	#MAB1378 RRID:AB_2128317	
Anti-ITGA5 (1:100)	Abcam	#ab-150361 RRID:AB_2631309	
Anti-ITGAV (1:100)	Abcam	#ab-63490 RRID:AB_1140041	
Anti-COLIV (1:100)	Merck	#AB769 RRID:AB_92262	
Anti-LAMA1 (1:100)	T. Sasaki, Oita University	#1057+ RRID:NA	

Anti-LAMA4	Reagent/resource	Reference or source	Identifier or catalog number	
Ci-100		T. Sasaki, Oita University		
C1:100		T. Sasaki, Oita University		
RRID-AB_777178 RRID-AB_777178 RRID-AB_532379 Anti-YAP (1:00/ 1:200/1:1000) RRID-AB_532379 Anti-YAP (1:100/ 1:200/1:1000) Sigma		T. Sasaki, Oita University		
Anti-VAP (1:100 / 1:200 / 1:	Anti-Pdx1 (1:200)	Abcam		
1.200/t10000 Sigma		DSHB		
C1:1000 STAB C1:1000 C1:1000 C1:1000 C1:200		Cell Signaling		
C-200 RRID-AB_2255626		Sigma		
RRID:AB_10859908		DSHB		
RRID:AB_396079 million cell May 28002 RRID:AB_89363 May 28002 RRID:AB_893363 RRID:AB_893363 RRID:AB_893363 RRID:AB_893363 RRID:AB_893363 RRID:AB_893363 RRID:AB_893363 RRID:AB_893363 RRID:AB_1731941 RRID:AB_1731941 RRID:AB_1731941 RRID:AB_1731941 RRID:AB_1731941 RRID:AB_1731941 RRID:AB_2876633 RRID:AB_2876633 RRID:AB_2876633 RRID:AB_2876633 RRID:AB_2876633 RRID:AB_2891178 RRID:AB_2891178 PE IgG1, κ (5 μ/1 million cell) BD Biosciences May 296091 RRID:AB_2891178 PE IgG3, κ (1:200) BD Biosciences May 296091 RRID:AB_396091 RRID:AB_396091 RRID:AB_396091 RRID:AB_396091 RRID:AB_395142 RRID:AB_395142 RRID:AB_395142 RRID:AB_11160953		Cell Signaling		
RRID:AB_893363 RRID:AB_893363 RRID:AB_893363 RRID:CD49c (ITGA3) (5 µl/1 million cell) RRID:AB_1731941 RRID:AB_1731941 RRID:AB_1731941 RRID:AB_1731941 RRID:AB_1731941 RRID:AB_1731941 RRID:AB_1731941 RRID:AB_2876633 RRID:AB_287178 RRI	(ITGA6) (5 μl/1	BD Biosciences		
(ITGA3) (5 μl/1 million cell) Biolegend #327913 (RID:AB_2876633) APC anti-CD51 (ITGAV) (5 μl/1 million cell) Biolegend #400221 (RRID:AB_2891178) APC IgG2a, κ (5 μl/1 million cell) Biolegend #400221 (RRID:AB_2891178) PE IgG1, κ (5 μl/1 million cell or 10 μl/10 million cell) BD Biosciences #555749 (RID:AB_396091) APC IgG2b, κ (3 μl/1 million cell) Biolegend #4400311 (RRID:AB_396091) APC IgG2b, κ (1:200) BD Biosciences #553927 (RID:AB_395142) PE anti-GP2 (10 μl/10 million cells) Nordic Biosite #D277-5 (RID:AB_395142) PE anti-GP2 (10 μl/10 million cells) Proteintech #12949-1-AP (RID:AB_11160953) Anti-PDK4 (1:5000) Proteintech #12949-1-AP (RID:AB_2161499) Anti-vinculin (1:1000) Sigma #V9264 (RID:AB_228341) Goat anti-rabbit IgG (H + L) secondary antibody, HRP Thermo Fisher #31430 (RID:AB_228307) Goat anti-mouse IgG (H + L) secondary antibody, HRP Thermo Fisher #31430 (RID:AB_228307) Oligonucleotides and other sequence-based reagents Hs01076879_m1 Oligonucleotides and other sequence-based reagents Hs01076879_m1 ITGA3 TaqMan probe Thermo Fisher	(ITGA5) (3 µl/1	Biolegend		
(ITGAV) (5 μ /1 million cell) RRID:AB_2876633 APC IgG2a, κ (5 μ /1 million cell) Biolegend #400221 RRID:AB_2891178 PE IgG1, κ (5 μ /1 million cell or 10 μ /10 million cell) BD Biosciences #555749 RRID:AB_396091 APC IgG2b, κ (3 μ /1 million cell) Biolegend #400311 RRID:AB_2894969 PE IgG2a, κ (1:200) BD Biosciences #553927 RRID:AB_2894969 PE IgG2a, κ (1:200) BD Biosciences #553927 RRID:AB_395142 PE anti-GP2 (10 μ / Nordic Biosite #D277-5 RRID:AB_395142 PE anti-GP2 (10 μ / Nordic Biosite #12949-1-AP RRID:AB_1160953 Anti-PDK4 (1:5000) Proteintech #12949-1-AP RRID:AB_2161499 Anti-vinculin (1:1000) Sigma #V9264 RRID:AB_216603627 Goat anti-rabbit IgG (H + L) secondary antibody, HRP #31460 RRID:AB_228341 Goat anti-mouse IgG (H + L) secondary antibody, HRP #31430 RRID:AB_228307 Oligonucleotides and other sequence-based reagents #31430 RRID:AB_228307 Oligonucleotides and other sequence-based reagents Hs01076879_m1 ITGA3 TaqMan probe Thermo Fisher Hs01547673_m1 ITGA6 TaqMan probe Thermo Fisher Hs01041011_m1 ITGAV Taq	(ITGA3) (5 μl/1	Biolegend		
S μ/1 million cell RRID:AB_2891178	(ITGAV) (5 μl/1	Biolegend		
million cell or 10 μ/10 million cell) RRID:AB_396091 APC IgG2b, κ (3 μ/1 million cell) Biolegend #400311 RRID:AB_2894969 PE IgG2a, κ (1:200) BD Biosciences #553927 RRID:AB_395142 PE anti-GP2 (10 μl/ to million cells) Nordic Biosite #D277-5 RRID:AB_395142 PE anti-GP2 (10 μl/ to million cells) Proteintech #12949-1-AP RRID:AB_11160953 Anti-PDK4 (1:5000) Proteintech #12949-1-AP RRID:AB_2161499 Anti-vinculin (1:1000) Sigma #V9264 RRID:AB_2161499 Goat anti-rabbit IgG (H + L) secondary antibody, HRP Thermo Fisher #31460 RRID:AB_228341 Goat anti-mouse IgG (H + L) secondary antibody, HRP Thermo Fisher #31430 RRID:AB_228307 Oligonucleotides and other sequence-based reagents Hs02758991_g1 GAPDH TaqMan probe Thermo Fisher Hs01076879_m1 ITGAS TaqMan probe Thermo Fisher Hs01041011_m1 ITGA6 TaqMan probe Thermo Fisher Hs01041011_m1 ITGAV TaqMan Thermo Fisher Hs00233808_m1	APC IgG2a, κ (5 μl/1 million cell)	Biolegend		
RRID:AB_2894969 PE IgG2a, κ (1:200) BD Biosciences	million cell or 10 µl/10 million	BD Biosciences		
RRID:AB_395142		Biolegend		
10 million cells RRID:AB_11160953	PE IgG2a, κ (1:200)	BD Biosciences		
RRID:AB_2161499		Nordic Biosite		
Goat anti-rabbit IgG (H + L) secondary antibody, HRP Goat anti-mouse IgG (H + L) secondary antibody, HRP Goat anti-mouse IgG (H + L) secondary antibody, HRP Oligonucleotides and other sequence-based reagents GAPDH TaqMan Thermo Fisher Hs02758991_g1 ITGA3 TaqMan Thermo Fisher Hs01076879_m1 probe ITGA5 TaqMan Thermo Fisher Hs01547673_m1 probe ITGA6 TaqMan Thermo Fisher Hs01041011_m1 probe ITGAV TaqMan Thermo Fisher Hs00233808_m1		Proteintech		
IgG (H + L) secondary antibody, HRP Goat anti-mouse IgG (H + L) secondary antibody, HRP Oligonucleotides and other sequence-based reagents GAPDH TaqMan Thermo Fisher Hs01076879_m1 probe ITGA3 TaqMan Thermo Fisher Hs01547673_m1 probe ITGA6 TaqMan Thermo Fisher Hs01041011_m1 probe		Sigma		
IgG (H + L) secondary antibody, HRP Oligonucleotides and other sequence-based reagents GAPDH TaqMan Thermo Fisher Hs02758991_g1 ITGA3 TaqMan Thermo Fisher Hs01076879_m1 probe ITGA5 TaqMan Thermo Fisher Hs01547673_m1 probe ITGA6 TaqMan Thermo Fisher Hs01041011_m1 probe ITGAV TaqMan Thermo Fisher Hs00233808_m1	IgG (H + L) secondary	Thermo Fisher		
GAPDH TaqMan Thermo Fisher Hs02758991_g1 ITGA3 TaqMan Thermo Fisher Hs01076879_m1 ITGA5 TaqMan Thermo Fisher Hs01547673_m1 probe ITGA6 TaqMan Thermo Fisher Hs01041011_m1 ITGAV TaqMan Thermo Fisher Hs00233808_m1	IgG (H + L) secondary	Thermo Fisher		
probe ITGA3 TaqMan				
probe ITGA5 TaqMan Thermo Fisher Hs01547673_m1 probe ITGA6 TaqMan Thermo Fisher Hs01041011_m1 ITGAV TaqMan Thermo Fisher Hs00233808_m1		Thermo Fisher	Hs02758991_g1	
probe ITGA6 TaqMan probe Thermo Fisher Hs01041011_m1 ITGAV TaqMan Thermo Fisher Hs00233808_m1		Thermo Fisher	Hs01076879_m1	
probe ITGAV TaqMan Thermo Fisher Hs00233808_m1		Thermo Fisher	Hs01547673_m1	
_		Thermo Fisher	Hs01041011_m1	
		Thermo Fisher	Hs00233808_m1	

Reagent/resource	Reference or source	Identifier or catalog number
PDX1 TaqMan	Thermo Fisher	Hs00236830_m1
NEUROG3 TaqMan probe	Thermo Fisher	Hs01875204_s1
NEUROD1 TaqMan probe	Thermo Fisher	Hs00159598_m1
INS TaqMan probe	Thermo Fisher	Hs02741908_m1
GCG TaqMan probe	Thermo Fisher	Hs01031536_m1
CYR61 TaqMan probe	Thermo Fisher	Hs00155479_m1
CTGF TaqMan probe	Thermo Fisher	Hs01026927_g1
RPL37A TaqMan probe	Thermo Fisher	Hs01102345_m1
PDK4 TaqMan probe	Thermo Fisher	Hs01037712_m1
PDK4 siRNA	Thermo Fisher	s10262
ITGA3 siRNA	Thermo Fisher	s7541
ITGA6 siRNA	Thermo Fisher	s7494
Negative control siRNA	Thermo Fisher	#4392420
Chemicals, enzyme	s and other reagents	
CHIR99021	Axon Medchem	#1386
Activin A	PeproTech	#120-14
FGF2	PeproTech	#100-18B
Retinoic acid	Sigma Aldrich	#R2625
ТВР	Calbiochem	#565740
ALK5iII	Santa Cruz	#sc-221234A
Noggin	PeproTech	#120-10 C
Nicotinamide	Sigma Aldrich	#481907
Forskolin	Sigma Aldrich	#F6886
Latrunculin B	Sigma Aldrich	#L5288
Bovine serum albumin (BSA)	Sigma Aldrich	#B4287
Y-27632	Merck	#688000
Biolaminin 521 LN (LN521)	BioLamina	#LN521-05
Biolaminin 411 LN (LN411)	BioLamina	#LN411-02
B27 supplement minus Insulin	Thermo Fisher	#A1895601
B27 supplement	Thermo Fisher	#17504001
NutriStem hPSC XF, xeno-free medium	Sartorius	#05-100-1 A
StemPro [™] Accutase [™]	Thermo Fisher	#A1110501
Fibronectin (cell experiments)	Sigma	#F0895
Fibronectin (explant experiments)	Life Technologies	#33010-018
M-199 Media + phenol red	Thermo Fisher	#31150022
Lipofectamine 2000	Invitrogen	#11668019
Lipofectamine RNAiMax	Invitrogen	#13778100

Reagent/resource	Reference or source	Identifier or catalog number
SuperScript III	Thermo Fisher	#18080085
RIPA buffer	Thermo Fisher	#8990
Laemmli reducing SDS buffer	Thermo Fisher	#J60015.AC
Protease inhibitor	Thermo Fisher	#A32953
Software		
Adobe Illustrator 2023	Adobe	
Fiji 2.0/ImageJ	http://imagej.nih.gov/ij NIH Image	
Venny 2.1.0	https://bioinfogp.cnb.csic.es/tools/ venny/ Oliveros, 2007	
ILASTIK v1.4.0.post1	https://ilastik.org Berg et al, 2019	
GraphPad Prism 10	https://www.graphpad.com GraphPad	
FCS express 7	https://denovosoftware.com De Novo Software	
RStudio	https://posit.co/downloads/ RStudio	
R package DESeq2 v1.34.0	https://bioconductor.org/packages/ release/bioc/html/DESeq2.html Love et al, 2014	
R package MAST v1.30.0	Finak et al, 2015	
R package Seurat v5.3.0	https://cran.r-project.org/web/ packages/Seurat/index.html Hao et al, 2023	
STAR v2.7.2 d	https://github.com/alexdobin/STAR/ releases Dobin et al, 2013	
FastQC v0.11.9	http:// www.bioinformatics.babraham.ac.uk/ projects/fastqc Babraham Bioinformatics group	
multiqc v1.7	https://multiqc.info Ewels et al, 2016	
3DSuite	https://imagej.net/plugins/3d-imagej- suite/ Ollion et al, 2013	
Single-cell transcriptomic and spatial map of the human fetal pancreas Shiny App	https:// www.humanpancreasdevelopment.org/ (Olaniru et al, 2023)	
Other		
Ibidi μ-Slide 8 well ^{high} slides	Ibidi	#80806
Ibidi 12-well slides for imaging	Ibidi	#80801
Pierce™ BCA Protein Assay Kit	Thermo Fisher	#23227
RNeasy Micro Kit	Qiagen	#74004
RNeasy Mini Kit	Qiagen	#74106
iScript cDNA Synthesis Kit	BIO-RAD	#1708891
Applied Biosystems TaqMan Fast Universal PCR Master Mix (2X), no AmpErase UNG	Thermo Fisher	#4352042

Reagent/resource	Reference or source	Identifier or catalog number
NEBNext Ultra II RNA Library Prep Kit for Illumina	Bionordika	#E777OS
NEBNext Poly(A) mRNA Magnetic Isolation Module	Bionordika	#E7490S
LIVE/DEAD™ Fixable Violet Dead Cell Stain Kit	Thermo Fisher	#L34964
A647 Phalloidin	Thermo Fisher	#A22287
8-16% polyacrylamide gels	Bio-Rad	#4561105
Chemiluminescent HRP substrate kit	Thermo Fisher	#34579
Acetyl-CoA ELISA kit	Biomol	#G-AEES00006.96
Zeiss LSM 780	Zeiss	
Leica Microsystems DM- IL-LED microscope	Leica Microsystems	
QuantStudio 7 Flex	Applied Biosystems	
StepOne plus real- time qPCR system	Applied Biosystems	
Illumina NextSeq 2000	Illumina	
Illumina NextSeq 500	Illumina	
BD LSRFortessa	BD Biosciences	
Sony SH800	Sony	
BD FACS Aria III	BD Biosciences	
Varioskant™ LUX Multimode Microplate Reader	Thermo Fisher	

Methods and protocols

Stem cell culture and directed differentiation

HUES4 and NGN3-GFP-SA121 hESC cell lines were maintained on laminin-521 with daily changes of NutriStem medium at 37 °C and 5% CO₂. Cells were passaged two to three times weekly using Accutase at 80-90% confluency. The medium was supplemented with 10 µM ROCK inhibitor on the first day after passaging. Cells were seeded on laminin-521 for pancreatic differentiation at 80 K cells/cm². At 100% confluency, cells were induced to differentiate into pancreatic progenitor cells following a previously published protocol (Ameri et al, 2017). Treatments and reseeding were performed on day 19. Endocrine progenitors were generated by the addition of 0.5 µM latrunculin B from days 19-21 and culture until day 28. For reseeding, pancreatic progenitor cells were dissociated with accutase for 10 min at 37 °C and plated in Ibidi 8 or 12-well slides for imaging, or in 24-well plates for other analyses. In each case, the slides were precoated overnight at $4\,^{\circ}\text{C}$ with either 0.1 $\mu\text{g}/$ μl fibronectin or about 0.75 μg/cm² of indicated laminins.

For knockdown experiments, HUES4 cells (*ITGA3*, *ITGA6*) or NGN3-GFP cells (*PDK4*) were reseeded as described above. For knockdown of integrins, reseeded cells were plated on LN521-

coated 24-well plates with prepared siRNA-lipofectamine 2000 complexes. For knockdown of *PDK4*, cells were mixed with prepared siRNA-lipofectamine RNAiMax complexes and plated on LN411-coated 24-well plates. Transfected cells were harvested after 48 h for gene expression analysis.

Mouse work

Animal work was conducted at the Department of Experimental Medicine at Copenhagen University following the ethical regulations approved by the Danish animal inspectorate (Miljø- og fødevarelseministeriet—Dyrforsøgstilsynet, approval #2016-15-0201-01114) or at the animal facility at the IGBMC institute at Strasbourg University campus of Illkirch.

Itga3; Itga6 double knockout mice (De Arcangelis et al, 1999) were maintained on a heterozygous background due to embryonic lethality. Itga3^{+/-}; Itga6^{+/-} mice were intercrossed to generate the double mutants. Littermates lacking one integrin allele were considered wild type, Itga3^{+/-}; Itga6^{-/-} embryos were considered Itga6 single knockout, and Itga3^{-/-}; Itga6^{+/-} embryos were considered Itga3 single knockout.

Mice were kept on a C57BL/6 background. The day of vaginal plug was recorded as day 0.5 of gestation. Both male and female embryos were included in the experiments.

Ex vivo explant culture

The dorsal pancreata of E11.5 mouse embryos were microdissected and cultured (Percival and Slack, 1999) on ibidi $\mu\text{-Slide 8 well}^{high}$ slides precoated for 45 min with 0.1 $\mu g/\mu l$ fibronectin. The explant culture media was composed of M-199 media + phenol red supplemented with 10% fetal bovine serum (FBS), 1% penicillin/ streptomycin, and 0.5% Fungizone. The media was changed every other day. Explants were cultured at 37 °C for 3–4 days.

qPCR

RNA was extracted using either the RNeasy Mini kit or RNeasy Micro kit, depending on the expected RNA yield. In both cases, oncolumn DNAse treatment was performed. Reverse transcription was performed using either SuperScript III using 2.5 mM random hexamer and 2.5 mM oligo(dT) or using the iScript cDNA synthesis kit, in both cases according to the manufacturer's instructions.

Real-time quantitative PCR was conducted as either duplicates on a StepOne Plus Real-time qPCR system or as triplicates on a QuantStudio 7 Flex system using TaqMan Fast Universal PCR Master Mix. Relative gene expression was determined using either GAPDH or RPL37A.

RNA sequencing

RNA was extracted for qPCR analysis. RNA integrity was assessed using an Agilent Fragment Analyzer. Sequencing libraries were carried out according to the manufacturer's instructions using NEBNext Ultra II RNA Library Prep Kit for Illumina, along with the NEBNext Poly(A) mRNA Magnetic Isolation Module. Sequencing was run on an Illumina NextSeq 500 (latrunculin B-treated samples) or Illumina NextSeq 2000 (FN/LN411-exposed samples).

Fastq files were generated using bcl2fastq v2.20.0 and aligned to the hg38/ GRCh38.p13 genome using STAR (Dobin and Gingeras, 2015). Transcript expression levels were estimated with the --quantMode GeneCounts option and gencode.v32 annotations. FastQC was used for QC metrics, and multiqc (Ewels et al, 2016) for reporting. Data analysis was then performed with R/Bioconductor (R Core Team, 2021; Gentleman et al, 2004). Normalization and gene differential expression analysis were performed with DESeq2 (Love et al, 2014).

Sequencing datasets have been deposited to GEO.

Flow cytometry

Cells were dissociated using Accutase for 5-10 min at 37 °C and quenched with medium. Cells were then stained for 30 min on ice with LIVE/DEAD fixable violet. Cells were then either assayed directly for expression of NGN3-GFP, incubated with conjugated antibodies against surface markers or matched isotype controls for 1 h on ice prior to assay of NGN3-GFP and surface marker expression, or incubated for 20 min in 4% paraformaldehyde on ice for fixation. Fixed cells were washed with 1% BSA in PBS, and then incubated for 1 h on ice in permeabilization/blocking buffer [0.1% Triton X-100, 5% normal donkey serum (NDS)]. The cells were then incubated overnight at 4 °C with primary antibodies or isotype controls in blocking buffer. Cells were then washed and incubated for 1 h at room temperature with secondary antibodies. All secondary antibodies used were raised in donkey and purchased from Jackson Immunoresearch. Finally, cells were washed and resuspended in 1% BSA in PBS. All assays were performed on a BD LSRFortessa. Data was analyzed using FCS Express 7.

Fluorescently activated cell sorting

Pancreatic progenitor cells were differentiated until the late pancreatic progenitor stage (day 19), dissociated with Accutase for 5–10 min at 37 °C, and quenched with pancreatic progenitor stage medium. Cells were incubated with 5% (NDS) in PBS $^{-/-}$ for 45 min on ice for blocking. Next, cells were pelleted, resuspended in FACS buffer (0.1% bovine serum albumin (BSA), 2 mM EDTA, 10 μ M ROCK inhibitor Y-27632, and 50U Penicillin/Streptomycin in PBS $^{-/-}$) and incubated with mouse anti-GP2-PE for 1 h on ice. DAPI was used to stain dead cells. Cells were sorted on Sony SH800 or BD FACS Aria III cell sorters, with gating for live GP2high cells performed as described previously (Ameri et al, 2017). Cells were sorted into FACS buffer, pelleted, resuspended in pancreatic progenitor medium supplemented with 10 μ M Y-27632, and seeded at 50,000 cells/cm². Cells were cultured for 48 h before fixation or harvesting for subsequent analyses.

For analysis of sorted NGN3-GFP $^+$ cells, cells were sorted into NGN3-GFP $^+$ (GP2 high and NGN3-GFP $^+$ populations and were pelleted and harvested immediately.

Immunostaining and microscopy

For immunohistochemistry, mouse pancreata were dissected at E15.5, fixed, and sectioned as previously discussed (Kesavan et al, 2009). Tissues were sectioned at 20 μm using a Leica cryostat. Sections were dried for 15 min at 37 °C, washed in PBS $^{+/+}$ and incubated with blocking buffer (PBS $^{+/+}$ + 0.1% Triton X-100 + 5% NDS) for 3–4 h. Sections were then incubated with primary

antibodies in blocking buffer overnight at 4 °C in a humidified chamber. After washing, sections were incubated with secondary antibodies in blocking buffer for 1 h at RT. Sections were rewashed and mounted with fluorescent mounting medium. For staining of whole explants, a fixation of 30 min in 4% PFA at room temperature was followed by overnight blocking at 4 °C, three nights of incubation with primary antibodies at 4 °C, and overnight incubation with secondary antibodies at 4 °C.

In vitro generated cells were permeabilized at room temperature for 15 min in permeabilization buffer (PBS^{+/+} + 0.5% Triton X-100), followed by blocking for 1 h with blocking buffer and overnight incubation with primary antibodies in blocking buffer. Samples were then washed three times in washing buffer (PBS^{+/+} + 0.1% Triton X-100) and incubated for 1 h at room temperature with secondary antibodies and, in indicated samples, phalloidin. Cells were then washed three times in washing buffer, with DAPI added in the penultimate washing step.

Confocal images were acquired using a Zeiss laser scanning microscope (LSM 780) using Plan-Apochromat 20X/0.8 M27 and Plan-Apochromat 40X/1.20 water immersion objectives or Leica SP8 using HC PL APO CS2 20X/0.75 IMM objective. Tilescan images of the whole pancreatic explant area were acquired using a 20X/0.8 M27 objective. Images were stitched using Zen software and quantified for insulin and glucagon using Fiji. Insulin and glucagon ratios were measured by normalizing the integrated density, which considers the area and the mean gray value, of insulin and glucagon against the integrated density of E-cadherin. Brightfield and epifluorescence images were acquired using a Leica Microsystems DM-IL-LED microscope. For images presented in Figs. 4D, 6A, EV5E, and EV6A, the subtract background function in FIJI was applied with a rolling ball radius of 1000 pixels.

Time-lapse imaging was done on Zeiss LSM 780 using Plan-Apochromat 20X/0.8 M27. HUES4 cells were reseeded on LN411 or FN and incubated in a pre-heated humidified chamber (37 °C, 5% $\rm CO_2$). Imaging was started 1 h after reseeding. Z-stacks of differential-interference contrast (DIC) were acquired for each marked position every 15 min for 24 h.

Quantification of nuclear YAP expression

NKX6-1 nuclei were segmented using a random forest classifier trained using sparse annotations in Ilastik (Berg et al, 2019). All possible features were enabled. After obtaining an image mask, YAP intensity in the segmented nuclei was quantified three-dimensionally using 3D suite in FIJI (Ollion et al, 2013).

Western blotting

Cells were washed twice, collected, and lysed on ice for 30 min using RIPA buffer. Lysate was then sonicated for 1 min at 5 s intervals and centrifuged at $10,000 \times g$ at 4 °C, after which the supernatant was transferred into new tubes. Concentration was determined by bicinchoninic acid, and protein samples were boiled for 5 min in Laemmli reducing SDS buffer. Samples were separated by SDS-PAGE on 8–16% polyacrylamide gels and transferred to PVDF membranes. Membranes were blocked for 1 h at room temperature in a blocking buffer consisting of 3% non-fat milk in TBS and incubated overnight with primary antibodies in the same blocking buffer. After washing,

membranes were incubated for 1 h at room temperature with horse-radish peroxidase-conjugated secondary antibodies. Bands were detected by a chemiluminescent HRP substrate kit. Bands were then quantified by densitometry using FIJI.

Acetyl-CoA measurement by ELISA

Cells were washed once with PBS and lysed on ice for 10 min in lysis buffer containing 0.5% NP-40, 50 mM Tris-HCl (pH 7.4), 150 mM NaCl, 1 mM EDTA and 1 × Protease inhibitor. Lysates were centrifuged at $10,000 \times g$ for 10 min at 4 °C to remove debris. The supernatant was collected and immediately used or stored at -80 °C. Acetyl-CoA levels were quantified using the acetyl-CoA ELISA kit following the manufacturer's protocol. Samples and standards were measured in duplicates, and absorbance was recorded at 450 nm using the VarioskantTM LUX Multimode Microplate Reader. Final concentrations were normalized to total protein content determined by BCA assay.

Single-cell RNA-seq data analysis

The OMIX001616 dataset (Ma et al, 2023), containing human fetal pancreata from weeks 4–11 post conception, was downloaded from the CNCB website. Analysis was restricted to 8–10 wpc and previously annotated "Trunk" and "EP" (endocrine progenitor) populations. Data processing was performed using R with Seurat v5.3.0. Statistical analysis was performed using MAST v1.30.0, with p-values adjusted using the Benjamini–Hochberg method to account for multiple comparisons. Expression of laminin α isoforms was assessed using the Shiny app at humanpancreasdevelopment.org (Olaniru et al, 2023).

Statistical analysis

Statistical analyses were performed using GraphPad Prism version 10. Two-sample comparisons were performed using two-tailed Student's t-tests. When possible, pairing according to the differentiation batch was performed. In other cases, Welch's t-test was employed. Experiments with more than two samples were analyzed by one-way repeated measures ANOVA with Geisser-Greenhouse correction, followed by Dunnett's multiple comparison test. For ELISA analysis of acetyl-CoA levels, two-way repeated measures ANOVA was performed with Geisser-Greenhouse correction, followed by Dunnett's test. Significance was defined as p < 0.05. Exact p values are shown on graphs unless p < 0.0001.

Data availability

The RNA sequencing data generated in this study has been deposited in the Gene Expression Omnibus (GEO) under accession codes GSE275775 (latrunculin B- and DMSO-treated samples) and GSE279067 (FN/LN411-exposed samples).

The source data of this paper are collected in the following database record: biostudies:S-SCDT-10_1038-S44319-025-00610-6.

Expanded view data, supplementary information, appendices are available for this paper at https://doi.org/10.1038/s44319-025-00610-6.

Peer review information

A peer review file is available at https://doi.org/10.1038/s44319-025-00610-6

References

- Ahnfelt-Rønne J, Jørgensen MC, Klinck R, Jensen JN, Füchtbauer EM, Deering T, MacDonald RJ, Wright CVE, Madsen OD, Serup P (2012) Ptf1a-mediated control of Dll1 reveals an alternative to the lateral inhibition mechanism. Development 139:33-45
- Ameri J, Borup R, Prawiro C, Ramond C, Schachter KA, Scharfmann R, Semb H (2017) Efficient generation of glucose-responsive beta cells from isolated GP2+ human pancreatic progenitors. Cell Rep 19:36-49
- Apelqvist Å, Li H, Sommer L, Beatus P, Anderson DJ, Honjo T, Hrabě De Angelis M, Lendahl U, Edlund H (1999) Notch signalling controls pancreatic cell differentiation. Nature 400:877-881
- Asp M, Giacomello S, Larsson L, Wu C, Fürth D, Qian X, Wärdell E, Custodio J, Reimegård J, Salmén F et al (2019) A spatiotemporal organ-wide gene expression and cell atlas of the developing human heart. Cell 179:1647-1660.e19
- Azzolin L, Panciera T, Soligo S, Enzo E, Bicciato S, Dupont S, Bresolin S, Frasson C, Basso G, Guzzardo V et al (2014) YAP/TAZ incorporation in the β -catenin destruction complex orchestrates the Wnt response. Cell 158:157–170
- Berg S, Kutra D, Kroeger T, Straehle CN, Kausler BX, Haubold C, Schiegg M, Ales J, Beier T, Rudy M et al (2019) ilastik: interactive machine learning for (bio) image analysis. Nat Methods 16:1226-1232
- Calvo F, Ranftl R, Hooper S, Farrugia AJ, Moeendarbary E, Bruckbauer A, Batista F, Charras G, Sahai E (2015) Cdc42EP3/BORG2 and septin network enables mechano-transduction and the emergence of cancer-associated fibroblasts. Cell Rep 13:2699-2714
- Cao D, Bergmann J, Zhong L, Hemalatha A, Dingare C, Jensen T, Cox AL, Greco V, Steventon B, Sozen B (2024) Selective utilization of glucose metabolism guides mammalian gastrulation. Nature 2024:1-10
- Cebola I, Rodríguez-Seguí SA, Cho CHH, Bessa J, Rovira M, Luengo M,
 Chhatriwala M, Berry A, Ponsa-Cobas J, Maestro MA et al (2015) TEAD and
 YAP regulate the enhancer network of human embryonic pancreatic
 progenitors. Nat Cell Biol 17:615-626
- Chi F, Sharpley MS, Nagaraj R, Roy SS, Banerjee U (2020) Glycolysis-independent glucose metabolism distinguishes TE from ICM fate during mammalian embryogenesis. Dev Cell 53:9-26.e4
- De Arcangelis A, Mark M, Kreidberg J, Sorokin L, Georges-Labouesse E (1999) Synergistic activities of $\alpha 3$ and $\alpha 6$ integrins are required during apical ectodermal ridge formation and organogenesis in the mouse. Development 126:3957–3968
- Dingare C, Cao D, Yang JJ, Sozen B & Steventon B (2024) Mannose controls mesoderm specification and symmetry breaking in mouse gastruloids. Dev Cell 591523-1537
- Dobin A, Davis CA, Schlesinger F, Drenkow J, Zaleski C, Jha S, Batut P, Chaisson M, Gingeras TR (2013) STAR: ultrafast universal RNA-seq aligner. Bioinformatics 29:15
- Dobin A, Gingeras TR (2015) Mapping RNA-seq reads with STAR. Curr Protoc Bioinformatics 51:11.14.1-11.14.19
- Du J, Chen X, Liang X, Zhang G, Xu J, He L, Zhan Q, Feng XQ, Chien S, Yang C (2011) Integrin activation and internalization on soft ECM as a mechanism of induction of stem cell differentiation by ECM elasticity. Proc Natl Acad Sci USA 108:9466-9471
- Engel-Pizcueta C, Pujades C (2021) Interplay between Notch and YAP/TAZ pathways in the regulation of cell fate during embryo development. Front Cell Dev Biol 9:711531

Ewels P, Magnusson M, Lundin S, Käller M (2016) MultiQC: summarize analysis results for multiple tools and samples in a single report. Bioinformatics 32:3047-3048

- Finak G, McDavid A, Yajima M, Deng J, Gersuk V, Shalek AK, Slichter CK, Miller HW, McElrath MJ, Prlic M et al (2015) MAST: a flexible statistical framework for assessing transcriptional changes and characterizing heterogeneity in single-cell RNA sequencing data. Genome Biol 16:1-13
- Frieser M, Nöckel H, Pausch F, Röder C, Hahn A, Deutzmann R, Sorokin LM (1997) Cloning of the mouse laminin α4 cDNA. Expression in a subset of Endothelium. Eur J Biochem 246:727–735
- Fujitani Y, Fujitani S, Boyer DF, Gannon M, Kawaguchi Y, Ray M, Shiota M, Stein RW, Magnuson MA, Wright CVE (2006) Targeted deletion of a cis-regulatory region reveals differential gene dosage requirements for Pdx1 in foregut organ differentiation and pancreas formation. Genes Dev 20:253-266
- Gao T, Zhou D, Yang C, Singh T, Penzo-Méndez A, Maddipati R, Tzatsos A, Bardeesy N, Avruch J, Stanger BZ (2013) Hippo signaling regulates differentiation and maintenance in the exocrine pancreas. Gastroenterology 144:1543-1553 e1
- Gentleman RC, Carey VJ, Bates DM, Bolstad B, Dettling M, Dudoit S, Ellis B, Gautier L, Ge Y, Gentry J et al (2004) Bioconductor: open software development for computational biology and bioinformatics. Genome Biol 5:1-16
- Gradwohl G, Dierich A, LeMeur M, Guillemot F (2000) neurogenin3 is required for the development of the four endocrine cell lineages of the pancreas. Proc Natl Acad Sci USA 97:1607–1611
- Grassian AR, Metallo CM, Coloff JL, Stephanopoulos G, Brugge JS (2011) Erk regulation of pyruvate dehydrogenase flux through PDK4 modulates cell proliferation. Genes Dev 25:1716-1733
- Gu G, Dubauskaite J, Melton DA (2002) Direct evidence for the pancreatic lineage: NGN3+ cells are islet progenitors and are distinct from duct progenitors. Development 129:2447-2457
- Hall ML, Givens S, Santosh N, Iacovino M, Kyba M, Ogle BM (2022) Laminin 411 mediates endothelial specification via multiple signaling axes that converge on β-catenin. Stem Cell Rep 17:569-583
- Hao Y, Stuart T, Kowalski MH, Choudhary S, Hoffman P, Hartman A, Srivastava A, Molla G, Madad S, Fernandez-Granda C, Satija R (2023) Dictionary learning for integrative, multimodal and scalable single-cell analysis. Nat Biotechnol 42:293-304
- Hogrebe NJ, Augsornworawat P, Maxwell KG, Velazco-Cruz L, Millman JR (2020)
 Targeting the cytoskeleton to direct pancreatic differentiation of human pluripotent stem cells. Nat Biotechnol 38:460-470
- Holness MJ, Sugden MC (2003) Regulation of pyruvate dehydrogenase complex activity by reversible phosphorylation. Biochem Soc Trans 31:1143-1151
- Ibar C, Irvine KD (2020) Integration of Hippo-YAP signaling with metabolism. Dev Cell 54:256-267
- Ishikawa T, Wondimu Z, Oikawa Y, Gentilcore G, Kiessling R, Egyhazi Brage S, Hansson J, Patarroyo M (2014) Laminins 411 and 421 differentially promote tumor cell migration via α6β1 integrin and MCAM (CD146). Matrix Biol 38:69–83
- Jensen J, Pedersen EE, Galante P, Hald J, Heller RS, Ishibashi M, Kageyama R, Guillemot F, Serup P, Madsen OD (2000) Control of endodermal endocrine development by Hes-1. Nat Genet 24:36-44
- Kao DI, Lacko LA, Ding BS, Huang C, Phung K, Gu G, Rafii S, Stuhlmann H, Chen S (2015) Endothelial cells control pancreatic cell fate at defined stages through EGFL7 signaling. Stem Cell Rep 4:181
- Kesavan G, Sand FW, Greiner TU, Johansson JK, Kobberup S, Wu X, Brakebusch C, Semb H (2009) Cdc42-mediated tubulogenesis controls cell specification. Cell 139:791-801

- La Manno G, Siletti K, Furlan A, Gyllborg D, Vinsland E, Mossi Albiach A, Mattsson Langseth C, Khven I, Lederer AR, Dratva LM et al (2021) Molecular architecture of the developing mouse brain. Nature 596:92-96
- Lammert E, Cleaver O, Melton D (2001) Induction of pancreatic differentiation by signals from blood vessels. Science 294:564–567
- Lee EH, Chung JW, Sung E, Yoon BH, Jeon M, Park S, Chun SY, Lee JN, Kim BS, Kim HT et al (2022a) Anti-metastatic effect of pyruvate dehydrogenase kinase 4 inhibition in bladder cancer via the ERK, SRC, and JNK pathways. Int J Mol Sci 23:13240
- Lee YB, Min JK, Kim JG, Cap KC, Islam R, Hossain AJ, Dogsom O, Hamza A, Mahmud S, Choi DR et al (2022b) Multiple functions of pyruvate kinase M2 in various cell types. J Cell Physiol 237:128-148
- Löf-Öhlin ZM, Nyeng P, Bechard ME, Hess K, Bankaitis E, Greiner TU, Ameri J, Wright CV, Semb H (2017) EGFR signalling controls cellular fate and pancreatic organogenesis by regulating apicobasal polarity. Nat Cell Biol 19:1313–1325
- Love MI, Huber W, Anders S (2014) Moderated estimation of fold change and dispersion for RNA-seq data with DESeq2. Genome Biol 15:550
- Lu Z, Hunter T (2018) Metabolic kinases moonlighting as protein kinases. Trends Biochem Sci 43:301-310
- Ma Z, Zhang X, Zhong W, Yi H, Chen X, Zhao Y, Ma Y, Song E, Xu T (2023)

 Deciphering early human pancreas development at the single-cell level. Nat

 Commun 14:1-17
- Magenheim J, Ilovich O, Lazarus A, Klochendler A, Ziv O, Werman R, Hija A, Cleaver O, Mishani E, Keshet E et al (2011) Blood vessels restrain pancreas branching, differentiation and growth. Development 138:4743-4752
- Mahmoud AI (2023) Metabolic switches during development and regeneration.

 Development 150:dev202008
- Mamidi A, Prawiro C, Seymour PA, de Lichtenberg KH, Jackson A, Serup P, Semb H (2018) Mechanosignalling via integrins directs fate decisions of pancreatic progenitors. Nature 564:114-118
- Miralles F, Czernichow P, Scharfmann R (1998) Follistatin regulates the relative proportions of endocrine versus exocrine tissue during pancreatic development. Development 125:1017–1024
- Nicolino M, Claiborn KC, Senée V, Boland A, Stoffers DA, Julier C (2010) A novel hypomorphic PDX1 mutation responsible for permanent neonatal diabetes with subclinical exocrine deficiency. Diabetes 59:733
- Ohta R, Niwa A, Taniguchi Y, Suzuki NM, Toga J, Yagi E, Saiki N, Nishinaka-Arai Y, Okada C, Watanabe A et al (2016) Laminin-guided highly efficient endothelial commitment from human pluripotent stem cells. Sci Rep 6:1-12
- Olaniru OE, Kadolsky U, Kannambath S, Vaikkinen H, Fung K, Dhami P, Persaud SJ (2023) Single-cell transcriptomic and spatial landscapes of the developing human pancreas. Cell Metab 35:184-199.e5
- Oliver-Krasinski JM, Kasner MT, Yang J, Crutchlow MF, Rustgi AK, Kaestner KH, Stoffers DA (2009) The diabetes gene Pdx1 regulates the transcriptional network of pancreatic endocrine progenitor cells in mice. J Clin Invest
- Oliveros JC (2007) VENNY. An interactive tool for comparing lists with Venn diagrams. http://bioinfogp.cnb.csic.es/tools/venny/index.html
- Ollion J, Cochennec J, Loll F, Escudé C, Boudier T (2013) TANGO: a generic tool for high-throughput 3D image analysis for studying nuclear organization. Bioinformatics 29:1840–1841
- Panciera T, Azzolin L, Cordenonsi M, Piccolo S (2017) Mechanobiology of YAP and TAZ in physiology and disease. Nat Rev Mol Cell Biol 18:758–770
- Percival AC, Slack JMW (1999) Analysis of pancreatic development using a cell lineage label. Exp Cell Res 247:123-132
- Pierreux CE, Cordi S, Hick AC, Achouri Y, Ruiz de Almodovar C, Prévot PP, Courtoy PJ, Carmeliet P, Lemaigre FP (2010) Epithelial: endothelial cross-talk regulates exocrine differentiation in developing pancreas. Dev Biol 347:216–227

Qu X, Afelik S, Jensen JN, Bukys MA, Kobberup S, Schmerr M, Xiao F, Nyeng P, Veronica Albertoni M, Grapin-Botton A et al (2013) Notch-mediated posttranslational control of Ngn3 protein stability regulates pancreatic patterning and cell fate commitment. Dev Biol 376:1-12

- R Core Team (2021) R: a language and environment for statistical computing. https://www.R-project.org/
- Romani P, Valcarcel-Jimenez L, Frezza C, Dupont S (2020) Crosstalk between mechanotransduction and metabolism. Nat Rev Mol Cell Biol 22:22–38
- Sakhneny L, Epshtein A, Landsman L (2021) Pericytes contribute to the islet basement membranes to promote beta-cell gene expression. Sci Rep 11:1-10
- Serafimidis I, Heximer S, Beis D, Gavalas A (2011) G protein-coupled receptor signaling and sphingosine-1-phosphate play a phylogenetically conserved role in endocrine pancreas morphogenesis. Mol Cell Biol 31:4442-4453
- Shibata S, Hayashi R, Okubo T, Kudo Y, Katayama T, Ishikawa Y, Toga J, Yagi E, Honma Y, Quantock AJ et al (2018) Selective laminin-directed differentiation of human induced pluripotent stem cells into distinct ocular lineages. Cell Rep 25:1668-1679.e5
- Smith SB, Qu HQ, Taleb N, Kishimoto NY, Scheel DW, Lu Y, Patch AM, Grabs R, Wang J, Lynn FC et al (2010) Rfx6 directs islet formation and insulin production in mice and humans. Nature 463:775-780
- Soyer J, Flasse L, Raffelsberger W, Beucher A, Orvain C, Peers B, Ravassard P, Vermot J, Voz ML, Mellitzer G et al (2010) Rfx6 is an Ngn3-dependent winged helix transcription factor required for pancreatic islet cell development. Development 137:203-212
- Spaeth JM, Hunter CS, Bonatakis L, Guo M, French CA, Slack I, Hara M, Fisher SE, Ferrer J, Morrisey EE et al (2015) The FOXP1, FOXP2 and FOXP4 transcription factors are required for islet alpha cell proliferation and function in mice. Diabetologia 58:1836-1844
- Tambe Y, Terado T, Kim CJ, Mukaisho KI, Yoshida S, Sugihara H, Tanaka H, Chida J, Kido H, Yamaji K et al (2019) Antitumor activity of potent pyruvate dehydrogenase kinase 4 inhibitors from plants in pancreatic cancer. Mol Carcinog 58:1726-1737
- Thoudam T, Chanda D, Sinam IS, Kim BG, Kim MJ, Oh CJ, Lee JY, Kim MJ, Park SY, Lee SY et al (2022) Noncanonical PDK4 action alters mitochondrial dynamics to affect the cellular respiratory status. Proc Natl Acad Sci USA 119:e2120157119
- Totaro A, Castellan M, Di Biagio D, Piccolo S (2018) Crosstalk between YAP/ TAZ and Notch signaling. Trends Cell Biol 28:560-573
- Wang RH, Xu X, Kim HS, Xiao Z, Deng CX (2013) SIRT1 deacetylates FOXA2 and is critical for Pdx1 transcription and β -cell formation. Int J Biol Sci 9:934
- Zhang S, Hulver MW, McMillan RP, Cline MA, Gilbert ER (2014) The pivotal role of pyruvate dehydrogenase kinases in metabolic flexibility. Nutr Metab 11:1-9
- Zhang X, Yi H, Ma Z, Zhao Y, Ma Y, Song E, Xu T (2025) Single-cell transcriptome analysis of in vivo and in vitro human pancreas development. Genes Dis 12:101573
- Zhu Z, Li QV, Lee K, Rosen BP, González F, Soh CL, Huangfu D (2016) Genome editing of lineage determinants in human pluripotent stem cells reveals mechanisms of pancreatic development and diabetes. Cell Stem Cell 18:755-768

Acknowledgements

We thank Anna Øster, Jette Larsen, and Diana Bach for her excellent technical support, Anna Månsson for helping with animal experiments, and Ivan Kulik for input and assistance with immunofluorescence experiments. We would further like to thank Gelo Dela Cruz and Paul van Dieken of the DanStem Flow Cytometry platform, Anup Shrestha and Jutta Bulkescher of the DanStem Imaging Platform, and Helen Neil, Heike Wollmann, Adrija Kalvisa, and Magali

Michaut of the DanStem Genomics Platform. All the work is supported by the European Union's Horizon 2020 research and innovation program (ISLET, no. 874839), the Novo Nordisk Foundation Center for Stem Cell Biology (DanStem) at the University of Copenhagen (NNF grant, NNF17CC0027852) and the Helmholtz Zentrum München.

Author contributions

Christine Ebeid: Conceptualization; Formal analysis; Investigation; Visualization; Methodology. Adam Rump: Conceptualization; Data curation; Formal analysis; Investigation; Visualization; Methodology; Writing—original draft; Writing—review and editing. Chenglei Tian: Conceptualization; Investigation; Visualization; Methodology; Writing—review and editing. Anant Mamidi: Conceptualization; Supervision; Investigation. Adèle De Arcangelis: Resources; Writing—review and editing. Gérard Gradwohl: Resources; Writing—review and editing. Henrik Semb: Conceptualization; Supervision; Funding acquisition; Methodology; Project administration; Writing—review and editing.

Source data underlying figure panels in this paper may have individual authorship assigned. Where available, figure panel/source data authorship is listed in the following database record: biostudies:S-SCDT-10_1038-S44319-025-00610-6.

Funding

Open Access funding enabled and organized by Projekt DEAL.

Disclosure and competing interests statement

The authors declare no competing interests.

Open Access This article is licensed under a Creative Commons Attribution 4.0 International License, which permits use, sharing, adaptation, distribution and reproduction in any medium or format, as long as you give appropriate credit to the original author(s) and the source, provide a link to the Creative Commons licence, and indicate if changes were made. The images or other third party material in this article are included in the article's Creative Commons licence, unless indicated otherwise in a credit line to the material. If material is not included in the article's Creative Commons licence and your intended use is not permitted by statutory regulation or exceeds the permitted use, you will need to obtain permission directly from the copyright holder. To view a copy of this licence, visit http://creativecommons.org/licenses/by/4.0/. Creative Commons Public Domain Dedication waiver http://creativecommons.org/publicdomain/zero/1.0/ applies to the data associated with this article, unless otherwise stated in a credit line to the data, but does not extend to the graphical or creative elements of illustrations, charts, or figures. This waiver removes legal barriers to the re-use and mining of research data. According to standard scholarly practice, it is recommended to provide appropriate citation and attribution whenever technically possible.

© The Author(s) 2025

Expanded View Figures



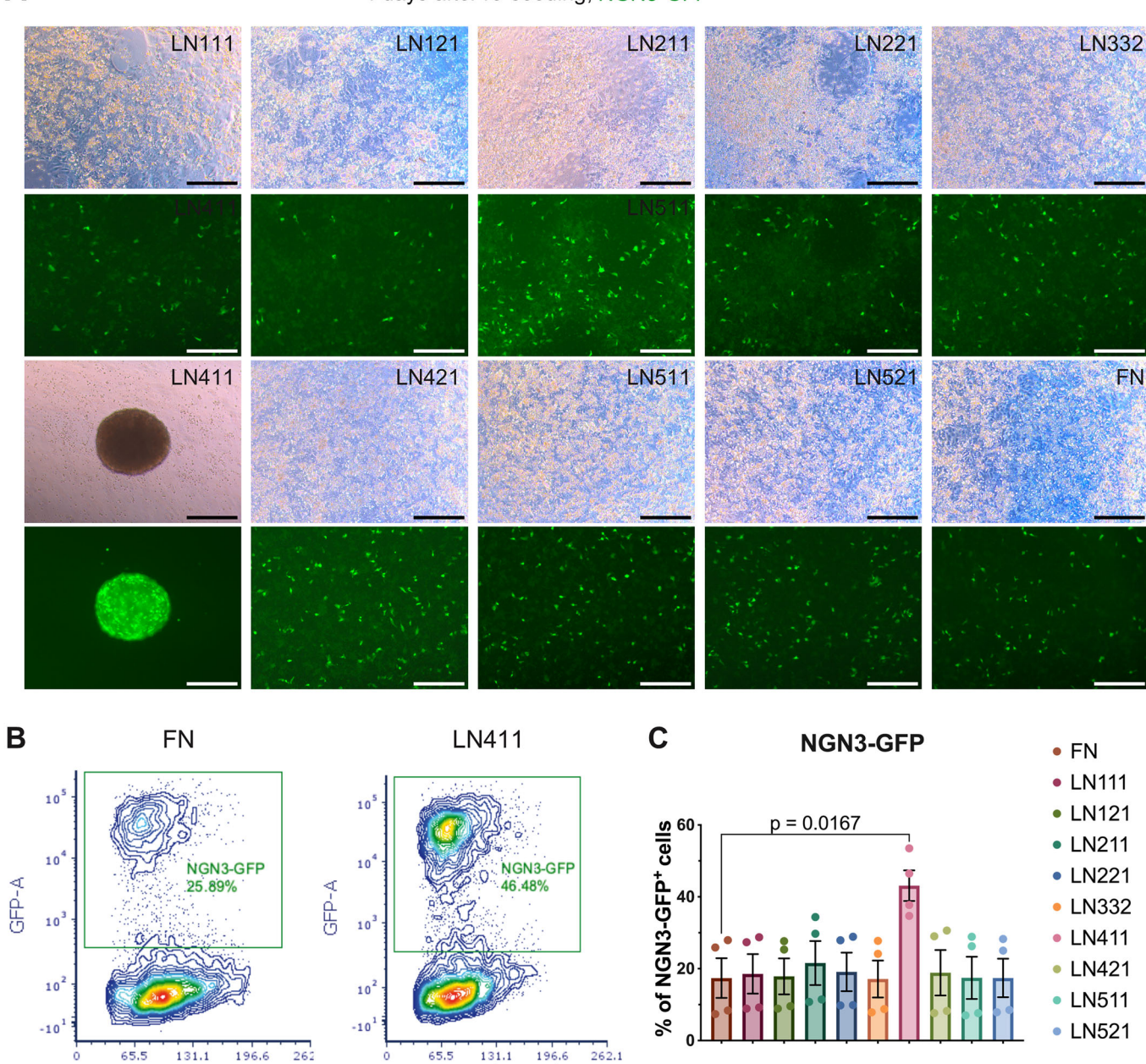


Figure EV1. LN411 specifically induces endocrine specification in the NGN3-GFP cell line.

FSC-A (x 1000)

(A) Representative brightfield (first and third row of panels) and epifluorescence (second and fourth row of panels) images of NGN3-GFP-derived pancreatic progenitors 4 days after reseeding on the indicated ECM proteins. Scale bar = $200 \,\mu\text{m}$. (B) Representative flow cytometry plots of NGN3-GFP reporter expression 4 days after reseeding. (C) Quantification of NGN3-GFP reporter expression in (B). The data were analyzed by Dunnett's test with comparison to FN and are shown as mean expression \pm SEM (n=4, biological replicates).

FSC-A (x 1000)

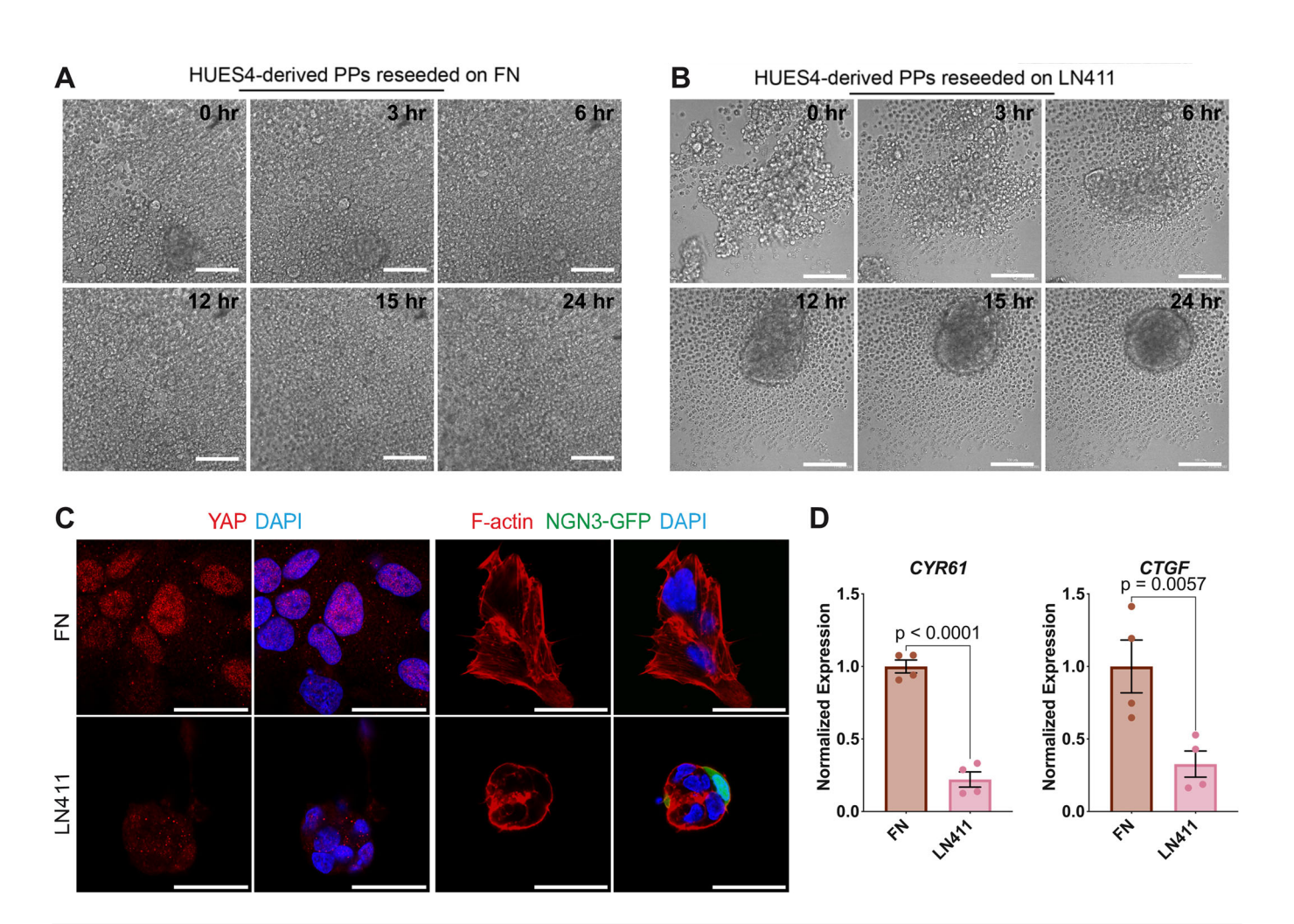


Figure EV2. LN411 induces a confined morphology, reduces actin polymerization, and decreases YAP activity.

(A) Live imaging of HUES4-derived pancreatic progenitors reseeded on FN by differential-interference contrast (DIC). Imaging started 1 h after reseeding. Scale bar = $100 \, \mu$ M. (B) Live imaging of HUES4-derived pancreatic progenitors reseeded on LN411 by differential-interference contrast (DIC). Imaging started 1 h after reseeding. Scale bar = $100 \, \mu$ M. (C) NGN3-GFP-derived pancreatic progenitors were sorted for GP2 using fluorescence-activated cell sorting, reseeded on FN (top panels) or LN411 (bottom panels) for 2 days and immunostained for YAP (left panels, red) or with phalloidin (right panels, red) in addition to DAPI (blue). Scale bar = $30 \, \mu$ m. (D) qPCR analysis of pancreatic of the YAP target genes *CYR61* and *CTGF* in NGN3-GFP derived pancreatic progenitors 24 h after reseeding on LN411 or FN. The data were analyzed using two-tailed paired t-tests and are shown as mean expression \pm SEM (n=4, biological replicates).

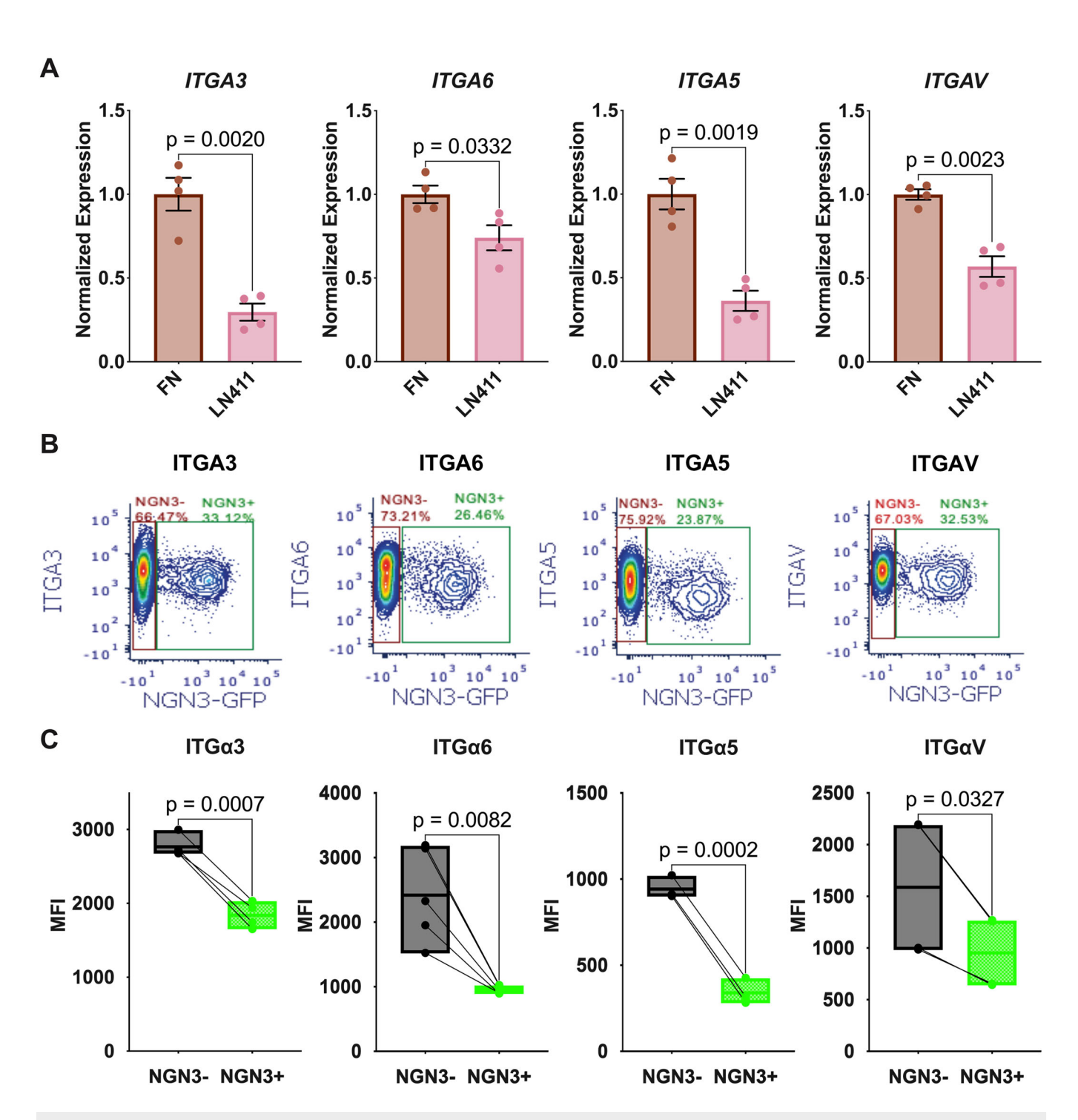


Figure EV3. Reseeding on LN411 leads to downregulation of integrins.

(A) qPCR analysis of indicated integrins in HUES4-derived pancreatic progenitors 4 days after reseeding on FN or LN411. The data were analyzed using two-tailed paired t-tests and are shown as mean expression \pm SEM (n=4, biological replicates). (B) Representative flow cytometry plots of Latrunculin B-treated NGN3-GFP-derived pancreatic progenitors immunostained for indicated integrins. (C) Quantification of mean fluorescence intensity in NGN3-GFP+ and NGN3-GFP- cells as indicated in (B). Data were analyzed by two-tailed paired t- and are shown as boxplots with box boundaries extending to the minimum and maximum with a line at the mean (n=4 for ITG α 3 and ITG α 6, n=3 for ITG α 7, biological replicates).

Christine Ebeid et al

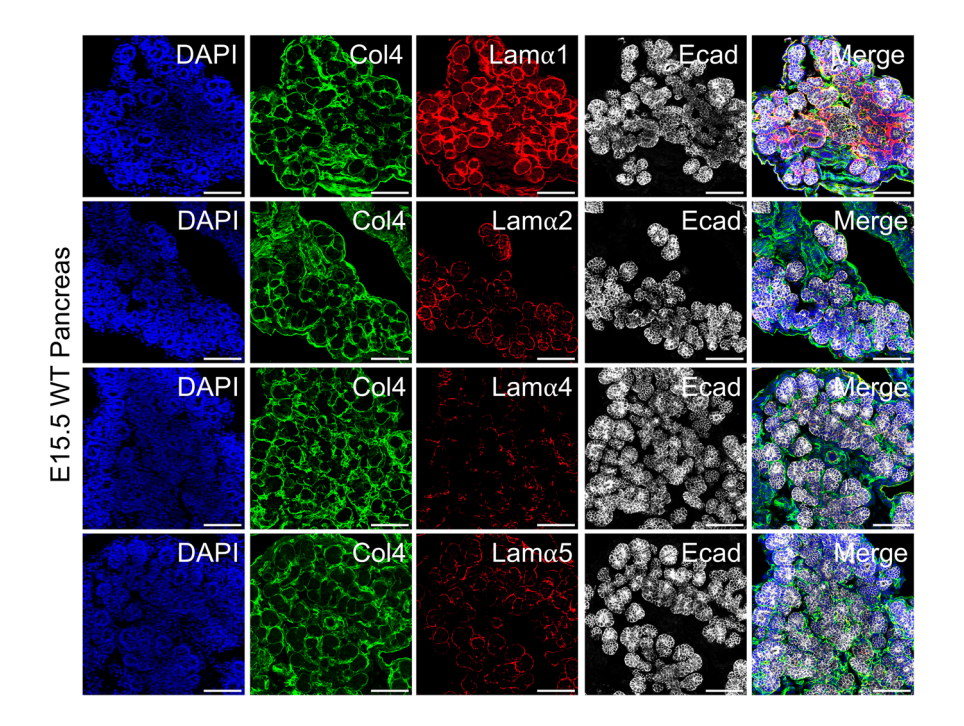
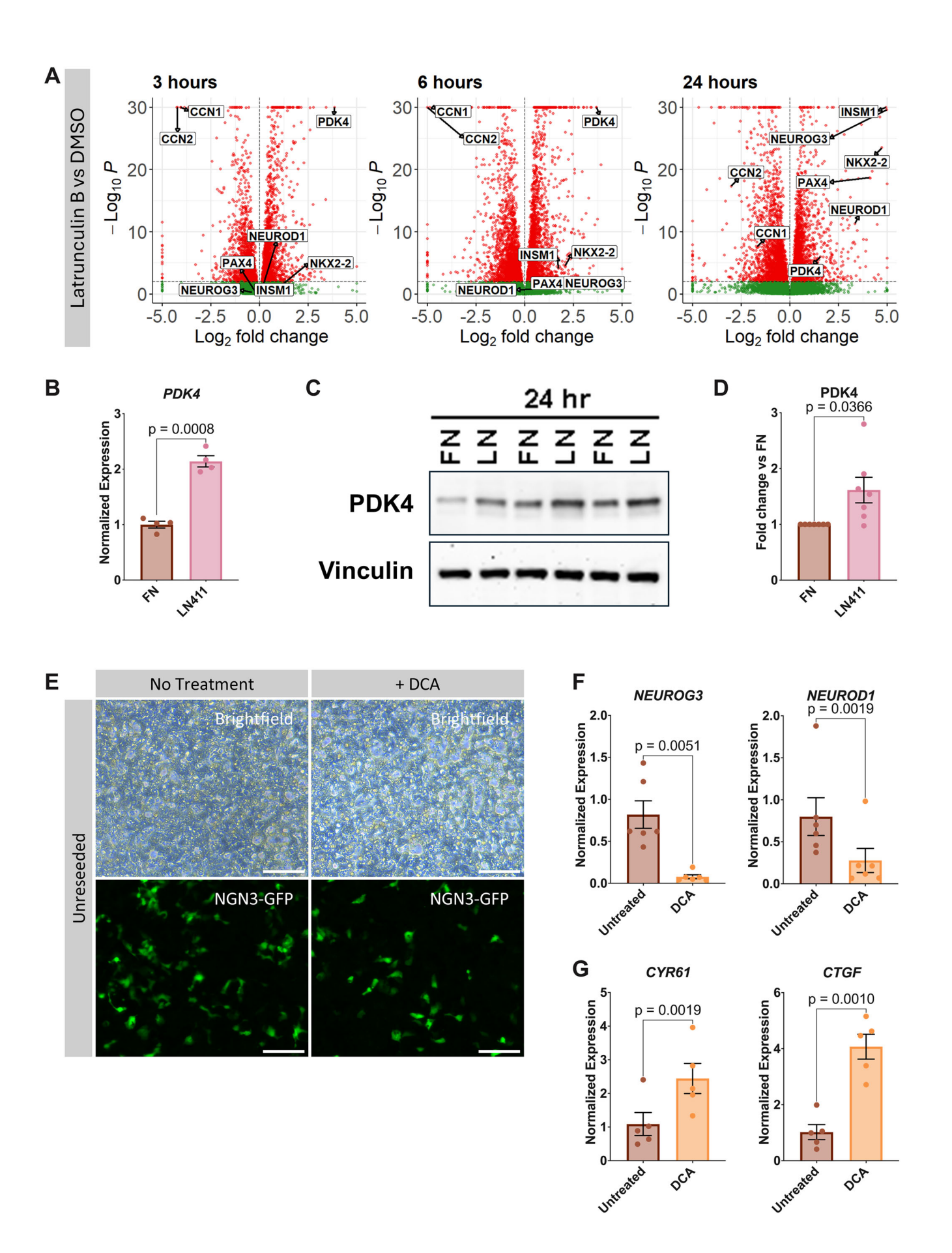


Figure EV4. Heterogenous expression of laminin isoforms in the pancreatic epithelium.

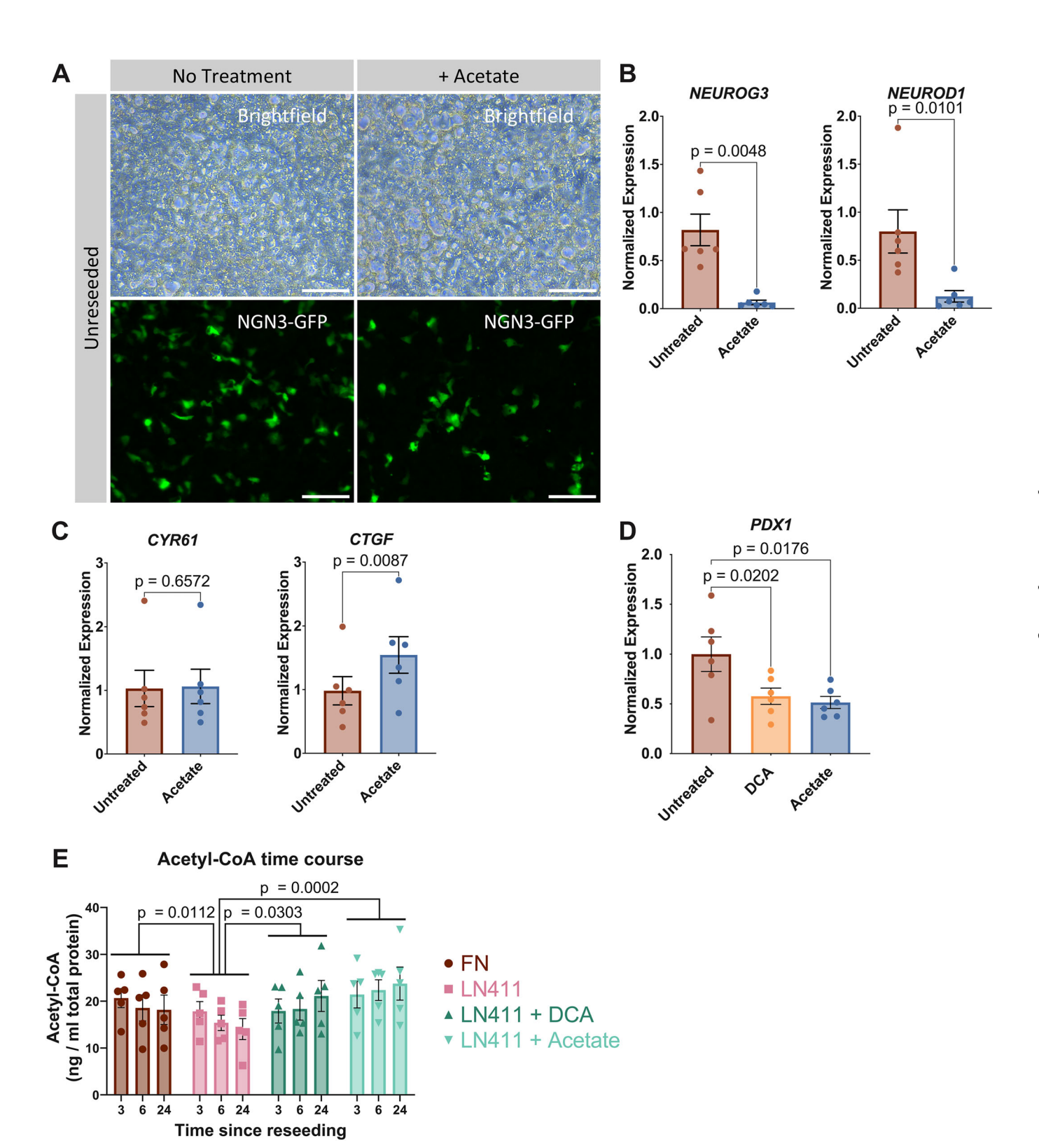
Immunofluorescent staining of 20- μ m sections of E15.5 pancreas immunostained for collagen IV (Col4, green), E-cadherin (E-cad, white), and indicated laminin α chains (Lam α 1-5, red), as well as DAPI (blue). Scale bar = 100 μ M.



23

■ Figure EV5. PDK4 upregulation precedes endocrine specification in non-reseeded pancreatic progenitors.

(A) Volcano plots of bulk RNA-seq analysis of NGN3-GFP-derived pancreatic progenitors treated with latrunculin B or DMSO at indicated time points. Expression of YAP target genes (CCN1/CYR61, CCN2/CTGF), early endocrine genes (NEUROG3, NEUROD1, INSM1, NKX2-2) and PDK4 are indicated. Differential expression analysis was performed using DESeq2 (n = 3). (B) qPCR analysis of PDK4 expression 24 h after reseeding on FN or LN411. The data were analyzed using two-tailed paired t-tests and are shown as mean expression \pm SEM (n = 4). (C) Western blot of PDK4 expression 24 h after reseeding on FN or LN411 (LN). Vinculin is included as a loading control. (D) Quantification of (C). The data were analyzed using two-tailed paired t-tests and are shown as mean expression \pm SEM (n = 7). (E) Brightfield (top panels) and epifluorescence (bottom panels) images of pancreatic progenitors after 2 days of no treatment or treatment with 10 mM DCA. Scale bar = 100 µm. (F) qPCR analysis of endocrine marker genes NEUROG3 and NEUROD1 in pancreatic progenitors after 2 days of no treatment or treatment with 10 mM DCA. The data were analyzed using two-tailed paired t-tests and are shown as mean expression \pm SEM (n = 6). (G) qPCR analysis of YAP target genes CYR61 and CTGF in pancreatic progenitors after 2 days of no treatment or treatment with 10 mM DCA. The data were analyzed using two-tailed paired t-tests and are shown as mean expression \pm SEM (n = 6).



■ Figure EV6. Acetate inhibits endocrine specification via a YAP-independent mechanism.

EMBO reports

(A) Brightfield (top panels) and epifluorescence (bottom panels) images of NGN3-GFP-derived pancreatic progenitors after 2 days of no treatment or treatment with 20 mM sodium acetate. Scale bar = $100 \, \mu m$. (B) qPCR analysis of endocrine marker genes *NEUROG3* and *NEUROD1* in pancreatic progenitors after 2 days of no treatment or treatment with 20 mM sodium acetate. The data were analyzed using two-tailed paired t-tests and are shown as mean expression \pm SEM (n = 6). (C) qPCR analysis of YAP target genes *CYR61* and *CTGF* in pancreatic progenitors after 2 days of no treatment or treatment with 20 mM sodium acetate. The data were analyzed using two-tailed paired t-tests and are shown as mean expression \pm SEM (n = 6). (D) qPCR analysis of *PDX1* in pancreatic progenitors after 2 days of no treatment with 10 mM DCA or 20 mM sodium acetate. The data were analyzed by Dunnett's test with comparison to the untreated condition and are shown as mean expression \pm SEM (n = 6). (E) ELISA analysis of intracellular acetyl-CoA concentrations in pancreatic progenitor cells at 3, 6, and 24 h after reseeding on FN, LN411, or LN411 with 10 mM DCA or 20 mM sodium acetate. The data were analyzed by two-way repeated measures ANOVA testing for treatment differences across the entire time course (3-24 h), followed by Dunnett's test with comparison to LN411 alone and are shown as mean expression \pm SEM (n = 5).

EMBO reports

Figure EV7. PDK4 induces endocrine fate choice via both canonical and non-canonical functions.

Schematic illustrating the proposed method of PDK4-mediated endocrine fate choice. Canonically, PDK4 blocks conversion of pyruvate to acetyl-CoA via inhibition of PDH (not shown). PDK4 additionally blocks YAP activity through a non-canonical mechanism. PDX1 is required for NGN3 expression, while YAP inhibits NGN3 expression. DCA targets PDK4 directly and thus increases YAP activity and decreases PDX1 expression. Acetate is converted to Acetyl-CoA, bypassing the effect of PDK4. Acetate treatment thus reduces PDX1 expression without affecting YAP activity.

Christine Ebeid et al

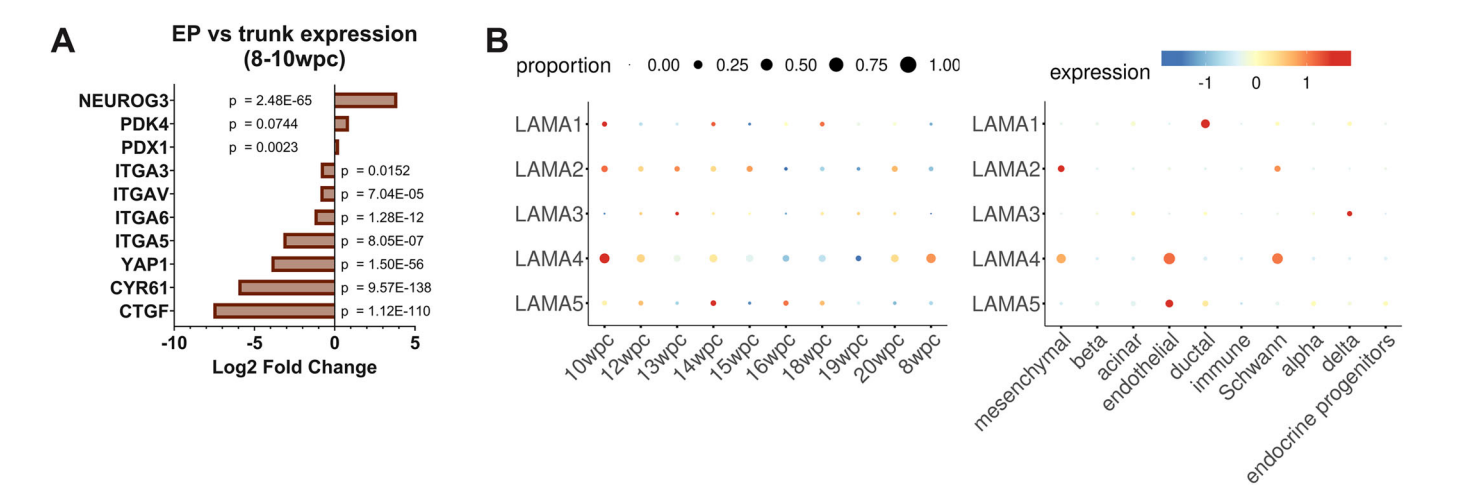


Figure EV8. Single-cell RNA sequencing datasets validate the LN411-PDK4-endocrine specification pathway.

(A) Log2 fold change in gene expression between endocrine progenitors (EP) and bipotent trunk progenitors (trunk) at 8-10 wpc in the OMIX001616 dataset (Ma et al, 2023). p-values are derived from MAST analysis (Finak et al, 2015) followed by Benjamini-Hochberg correction for multiple comparisons. (B) Dot plots of normalized expression of laminin α subunit genes in single-cell RNA sequencing samples of fetal pancreata according to developmental time (left) and cell type (right). Plots generated using humanpancreasdevelopment.org (Olaniru et al, 2023).